Open System Study of Conductance Quantization in 2D Chern Insulators

A Thesis

submitted to
Indian Institute of Science Education and Research Pune
in partial fulfillment of the requirements for the
BS-MS Dual Degree Programme

by

Satyam Sinha

Indian Institute of Science Education and Research Pune
Dr. Homi Bhabha Road,
Pashan, Pune 411008, INDIA.

April, 2025

Supervisor: Abhishek Dhar

Certificate

This is to certify that this dissertation entitled Open System Study of Conductance Quantization in 2D Chern Insulators towards the partial fulfilment of the BS-MS dual degree programme at the Indian Institute of Science Education and Research, Pune represents work carried out by Satyam Sinha at International Centre for Theoretical Sciences (ICTS), Bangalore under the supervision of Professor Abhishek Dhar, Department of Physics during the academic year 2024-2025.

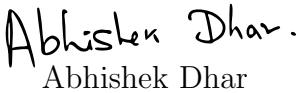

Abhishek Dhar

Committee:

Abhishek Dhar

Bijay Kumar Agarwalla

Sreejith G. J.

To every person and moment that sparked my growth and kept me moving forward.

Declaration

I hereby declare that the matter embodied in the report entitled Open System Study of Conductance Quantization in 2D Chern Insulators are the results of the work carried out by me at the Department of Physics, International Centre for Theoretical Sciences, Bangalore under the supervision of Professor Abhishek Dhar and the same has not been submitted elsewhere for any other degree.

Satyam Sinha

Acknowledgments

This thesis has been both achievable and enjoyable thanks to the guidance, knowledge and support I got from some truly amazing people. Firstly, I sincerely thank my supervisor, Prof. Abhishek Dhar, for giving me this great opportunity to work with him at ICTS. It has been an enriching and valuable experience engaging in discussions and exploring ideas under his guidance. Thank you so much for your time and patience. I am also grateful to my co-supervisor, Prof. Bijay Agarwalla, who kindly agreed to mentor me during the initial 3 months of my MS thesis at IISER Pune. His guidance in detailed understanding of prerequisite research papers played a crucial role in shaping my foundation for this project.

I would also like to extend my sincere thanks to Prof. R. Shankar (IMSc) for his invaluable guidance that was crucial to the analytical progress of the project. I am also grateful to Junaid Bhat and Rekha Kumari for their guidance and for always being there for a discussion about the project as well as other matters. The experience was all the more enjoyable thanks to both of you.

From IISER Pune, I am thankful to my mentors Prof. Sachin Jain and Prof. Deepak Dhar with whom doing research projects taught me to ask the right questions and understand the essence of quality research. Thanks also to many of my friends-Naman, Vivek, Ritesh, Garvit, and Aswini—from whom I have learned a great deal of physics. I also sincerely thanks them including my other friends, Rajat, Bhumika, Sweta, Chetan, and Harshit for being there at various crucial occasions and teaching me many little things that matter outside academics (which did indirectly had a positive impact on my MS project!)

At ICTS, I thank Abhinav Dhawan for several useful discussions and my other friends-Saikat, Abhinav, Kanak, Anjali, and Saiba for their constant support and companionship which made my time at ICTS feel like home, allowing me to consistently work on my thesis without burnouts. I am grateful to the entire ICTS community for fostering a friendly and

intellectually stimulating environment, and to the Long-Term Visiting Students Program at ICTS for funding my visit. I also acknowledge ChatGPT for assisting me with writing and debugging codes for simulations.

Lastly, but most importantly, I extend my heartfelt gratitude to my parents for their unwavering love and the sacrifices they have made for my education and well-being. I am especially thankful to my mother and sister for their constant encouragement and care—their support has been my greatest source of strength.

Abstract

This thesis aims to provide a microscopic understanding of the quantized conductance observed in experimental setups of 2D topological insulators (TIs), such as HgTe quantum wells, and in numerical simulations of corresponding microscopic models. These materials exhibit dissipationless edge transport in specific parameter regimes, with the quantization of two-terminal conductance serving as a key experimental signature of their topological nature.

Conductance measurements are typically performed in a Hall bar geometry, where the system is connected to metallic leads. The conventional explanation for the quantization of two-terminal conductance observed in 2D TI setups relies on the Landauer-Büttiker formalism, which equates it to the Hall conductance under two key assumptions: (i) there is effectively a single channel between the metallic leads and the system, and (ii) electron transmission at the metal-TI junction is perfect. However, it remains unclear why electron transmission should be perfect through this single channel regardless of the junction details. To the best of our knowledge, no analytical proof of these assumptions exists in the literature. In this work, we study a microscopic model of a Chern insulator coupled to metallic leads that closely mimics experimental transport setups. Using the non-equilibrium Green's function (NEGF) formalism, we analyze the roles of coupling and finite-size effects on the two-terminal conductance. Furthermore, by adopting a cylindrical geometry with idealized reservoirs, we derive an analytic expression for the Hall conductance in an integral form. The obtained expression is analytically shown to be quantized in the weak coupling limit. This integral turns out to be independent of coupling (even though the integrand depends on coupling) which suggests it's possible connection to a topological invariant similar to the TKNN expression (Thouless *et. al.* 1982) for closed periodic system where Hall conductivity is related to Chern number of filled bands.

Our results provide a theoretical foundation for understanding the quantization and robustness of conductance in an open system setup using NEGF. This study is a stepping stone towards bridging the gap between the experimentally measured two-terminal conductance and the theoretical concept of topological invariants, offering insights that could possibly guide the design of improved experimental setups for realizing 2D topological insulators.

Contents

Part I

Preliminaries and tools

Chapter 1

Introduction

1.1 Motivation and aim

Topological insulators (TIs) have garnered extensive attention in condensed matter physics community in the last two decades due to it's unusual metallic character and it's great potential for technological applications in electronic transport, spintronics and quantum computing [1]. In simplest language, Topological Insulators are special insulators whose boundaries can conduct electrons like metals. For example, if you have a Topological Insulator in form of a 2D rectangular slab and you apply a voltage bias, electrons can flow on the edges of the slab(but not in the bulk).

The origins of Topological condensed matter physics can be traced back to 1980, when von Klitzing *et al.* experimentally discovered that a 2D electron gas[1] subjected to strong magnetic field at low temperature shows an unusual and interesting transport feature [2]. Specifically, the Hall resistivity remains constant over finite intervals of the magnetic field, forming distinct plateaus before making abrupt jumps to the next quantized value (See figure 1.1). On these plateaus, the resistivity takes the form[2] :

$$\rho_{xy} = \frac{h}{e^2\nu} \quad \nu \in \mathbb{Z} \tag{1.1}$$

[1] 2D electron gas is obtained at the interface of a semiconductor heterojunction where electrons have high mobility.

[2] Note that in 2D, Hall resistance and Hall resistivity are equal. As a result, measuring Hall resistance is same as measuring Hall resistivity.

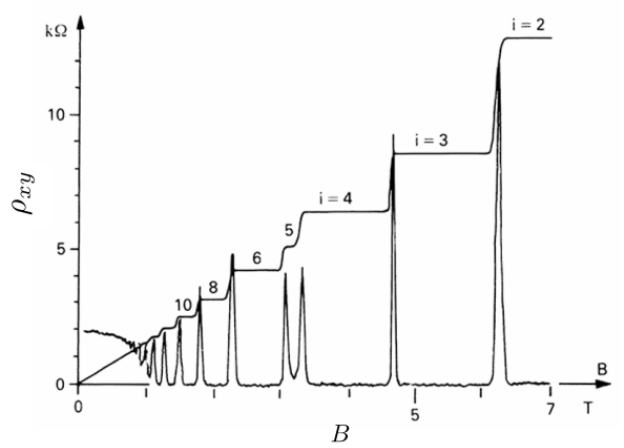

Figure 1.1: Experimental observation of the Integer Quantum Hall Effect. Note that the plot also includes longitudinal resistivity (ρ_{xx}) behaviour which peaks when there is jump in ρ_{xy} and remains zero elsewhere. This figure is taken from [3]

.

In other words, it was found that the Hall conductivity is quantized (in units of $\frac{e^2}{h}$). The measured value of ν was found to be an exact integer with remarkable precision—accurate to several decimal places[3]. This phenomenon is famously known as **Integer Quantum Hall Effect (IQHE)**. A theoretical explanation for this quantized conductance emerged through two foundational contributions.

A theoretical explanation for this quantized conductance arose through pioneering work by Laughlin [4] and the seminal 1982 study by Thouless, Kohmoto, Nightingale, and den Nijs (TKNN) [5]. Laughlin's argument, based on gauge invariance and adiabatic charge pumping, provided an early conceptual foundation for the robustness of the quantization. The TKNN framework later formalized this insight, demonstrating that the Hall conductivity of a 2D electron system in a periodic potential can be expressed as an integral of the Berry curvature over the Brillouin zone. This integral—a topological invariant called the Chern number—quantifies the global quantum geometry of the occupied electronic states. The TKNN result established that the IQHE is a bulk topological phenomenon, where the quantization of σ_{xy} arises from the non-local properties of the electron wavefunctions rather than local material details.

Shortly after the discovery of the Quantum Hall effect, researchers began to ask whether

[3]Consequently, quantum Hall effect experiments now serve as a metrological standard in the determination of the fine structure constant.

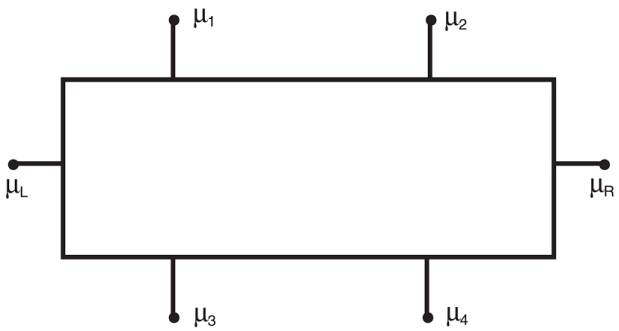

Figure 1.2: Hall Bar Geometry

similar topological features could exist in materials in the *absence* of an external magnetic field. Starting from the pioneering work of Haldane [6] and then Kane and Mele's work [7], it was soon realized that if *time-reversal symmetry (TRS)* is preserved and the spin-orbit coupling (SOC) is sufficiently large in the material, one could achieve a "quantum spin Hall" state. In 2006, Bernevig *et al* predicted the first experimentally realizable model for 2D Topological Insulator. They predicted that this new topological phase, characterized by a $\mathbb{Z}_2$ index, supports *helical* edge channels that likewise exhibit topological protection, though now the mechanism relies on TRS rather than an external magnetic field.

One of the experimental signature for the existence of this Topological Insulator is the quantization of two-terminal conductance [8]. However, note that the transport experiments for measuring conductance is done in a Hall bar geometry (see fig. 1.2) where the system (here, 2D Topological Insulator) is connected to metallic leads. The framework that connects the study of Topological Insulators(closed system setup) to Quantum Transport experiments (an open system setup) is the Landauer-Buttiker Formalism. Using this formalism with two extra assumptions, it can be shown that two-terminal conductance is equal to Hall conductance. The two assumptions taken can be stated as:

- There is an effectively a single channel between the Metallic lead and Chern Insulator.
- There is perfect transmission of electron from this single effective channel.

These assumptions are taken based on heuristic arguments about the 1D nature of edge states and their chiral nature. But, to the best of our understanding, no existing work provides an analytic proof showing that these two assumptions actually follows from a microscopic description.

The main goal of this study is to provide a microscopic, analytically grounded proof for why the electron can perfectly transmit through the Metal-Chern junction and what role does coupling plays in the quantization of conductance. Starting from a finite strip geometry setup of Chern Insulator connected to metallic leads, we explain how finite size effects in the conductance behaviour can be understood using non-hermitian Hamiltonian. Later we simplify our model by considering a cylindrical geometry and simplified reservoirs. We derive an expression for the Hall conductance in integral from suggesting a possible connection to some topological invariant. This could potentially help to clarify the link between the two terminal conductance (a experimentally measured quantity) and the theoretical concept of topological invariants.

1.1.1 Outline of the report

In chapter 2, we will start by reviewing some concepts related to topological insulators through a concrete example of a model: spinless BHZ, which is also the model of interest in this report.

In chapter 3, we discuss the formalism of Non-Equilibrium Green's function which is the framework in which we define our problem and try to obtain an analytic answer. The setup we consider is an open system setup: A 2D Chern insulator on a rectangular lattice connected to metallic leads at its ends. We briefly discuss this setup and it's special features that enable us to tackle the problem analytically. At the end, we briefly discuss transfer matrix, an analytical tool that helps to analytically go beyond formal expression of conductance in NEGF formalism.

In Chapter 4, we consider a strip geometry setup of Chern insulator connected to metallic leads. Using the effective non-Hermitian Hamiltonian obtained from the NEGF formalism, we explain some features of the numerically obtained plots for two-terminal conductance. We later discuss how understanding the non-hermitian Hamiltonian leads to a simpler model for reservoir which still captures quantization of conductance.

In chapter 5, we consider a cylindrical geometry setup. As the analytic calculation in the strip geometry became cumbersome due to lack of translational invariance, there was need to have further analytic simplifications. As a result, we consider cylindrical geometry, having translational invariance in y-direction. In this chapter, we discuss the need to define conductance in a different way because no current flows in the x-direction due to absence of

horizontal edges in the setup. We, then convert our 2D transport problem to an effective 1D transport problem by doing a Fourier transform along the $y-$direction. We then obtain a simple expression in the thermodynamic limit for the Hall conductance in an integral form. Evaluating this integral numerically shows that the Hall conductance is indeed quantized to 1, independent of the value of coupling. Further, we discuss here the nature of integrand for different values of coupling.

In Chapter 6, we discuss numerical results related to quantization of two-terminal conductance in Hofstadter model. We also discuss an interesting numerical result using a setup consisting only of nearest-neighbour tight binding model which shows similar current pattern to the one found in Chern Insulator Setups.

In Chapter 7,we conclude the report summarizing our main results and its implications.

Chapter 2

Topological insulators: A closed-system perspective

In this chapter, we will briefly overview some key concepts related to 2D topological insulators by considering the simplest possible example. Assuming translational symmetry in x and y directions, we will discuss about the meaning of bands having a non-trivial topology. Further we also discuss the role of the geometry of the material in real space and it's connection to the topology of bands.

2.1 What is a topological insulator?

Topological insulators (TIs) are special kind of insulators in which *disspationless* current can flow through its edges. This should be very surprising as realistic materials have a lattice structure and many impurities are also present which could cause scattering of electrons leading to energy loss. However, due to the significant contribution of spin-orbit coupling in the material from which TIs are made, the dispersion of the material has some special properties. This leads to "non-trivial topology" of band of the insulator. Such non-trivial topology of band implies the existence edge states whose energy lie in the band gap of the insulator. In the following sections, a brief overview of the key ideas related to the role of topology is presented using the simplest model for 2D topological insulator [9], i.e. Chern insulator on a square lattice.

2.1.1 Spinless BHZ (SBHZ): A model for 2D Chern insulator

The simplest model for topological insulator is the model of 2D Chern insulator on a square lattice. This model have it's origin from the pioneering paper on the quantum spin Hall effect, where it's authors predicted a material in which quantized hall conductance can be experimentally observed in the absence of magnetic field. This material can be modelled by BHZ (Bernevig-Hughes-Zhang) Hamiltonian. BHZ Hamiltonian in momentum space is given by:

$$H_{\text{BHZ}} = \begin{pmatrix} h(k) & 0 \\ 0 & h^*(-k) \end{pmatrix} \tag{2.1}$$

where,

$$h(k) = \sigma_x \, \text{sin}k_x + \sigma_y \, \text{sin}k_y + \sigma_z \, (\mu_w + \text{cos}k_x + \text{cos}k_y) \tag{2.2}$$

Since, the Hamiltonian is block diagonal this implies that we can uncouple the spin degrees of freedom and the internal degrees of freedom(due to spin-orbit coupling). This one copy of the Bloch Hamiltonian $h(k)$ is a Hamiltonian for **Chern insulator**. We will call it **spinless BHZ** Hamiltonian. So,

$$H_{\text{SBHZ}} = \sigma_x \, \text{sin}k_x + \sigma_y \, \text{sin}k_y + \sigma_z \, (\mu_w + \text{cos}k_x + \text{cos}k_y) = \mathbf{h}(\mathbf{k}) \cdot \boldsymbol{\sigma} \tag{2.3}$$

where $\boldsymbol{\sigma} = (\sigma_x, \sigma_y, \sigma_z)$ consists of 2×2 Pauli matrices. This Hamiltonian is a model for Chern insulator because it has a non-zero Chern number (a topological number to be defined in the next section). Hence, a 2D topological insulator can be seen as a set of two uncoupled 2D Chern insulator with opposite Chern number.

2.1.2 Momentum space topology

Before understanding the role of topology on the band structure, let us define a quantity called Chern number, which can be associated to each of the bands of an insulator:

$$\mathcal{C} = \frac{1}{4\pi} \int_{\mathcal{T}^2} d^2k \; \hat{\mathbf{h}} \cdot \left(\frac{\partial \hat{\mathbf{h}}}{\partial k_x} \times \frac{\partial \hat{\mathbf{h}}}{\partial k_y} \right) \tag{2.4}$$

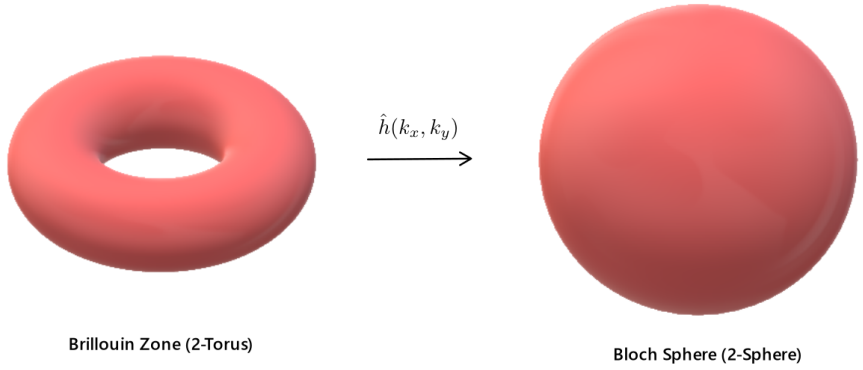

Figure 2.1: A map from 2-torus to 2-sphere

where,

$$\hat{\mathbf{h}} = \frac{\mathbf{h}(k)}{|\mathbf{h}(\mathbf{k})|} \tag{2.5}$$

Here, the integral is done over the Brillouin zone which is a 2-torus. Using some differential geometry arguments, it can be shown that the Chern number, $\mathcal{C}$ is always an integer. In fact, this integral has a nice physical interpretation. Note that, $\hat{\mathbf{h}}$ takes values from Brillouin zone (2-Torus) and gives a value on 2-sphere. Hence it is a map as shown in figure 2.1. So, this integral gives the no. of times the 2-torus wraps around 2-sphere [3]. Evaluating eq(2.4) using the dispersion $h(k)$ for spinless BHZ (SBHZ), one obtains the following result:

$$\mathcal{C} = \begin{cases} -1, & -2 < \mu_w < 0, \\ 1, & 0 < \mu_w < 2, \\ 0, & |\mu_w| > 2. \end{cases} \tag{2.6}$$

where μ_w is the parameter present in the SBHZ Hamiltonian (Eq. 2.3).

So, when $|\mu_w| < 2$, bands have a non-zero Chern number.

A non-zero Chern number implies a non-trivial topology of the band. From the bulk-boundary correspondence, a non-zero Chern number implies the existence of edge states in the band gap[[9]]. These states, arising from non-trivial topology, exist within the band gap and enable electron conduction even when the Fermi level is inside the band gap.

2.2 Role of setup geometry

Note that, in the previous section we wrote Hamiltonian in k-space. This requires that the lattice is translationally invariant, i.e. either the 2D lattice have periodic boundary condition or it extends to infinity in both direction. Without translational invariance, one cannot talk about the Bloch Hamiltonian and hence about the topology of bands. This constraint leads to difficulty in studying the physics of edge states.
It is very important to not get confused with the word *geometry* and *topology*. In the report, whenever we use the word geometry, it means the geometry of the lattice in the real-space. Following are the three typical geometry that would be relevant for our discussion:

- **Finite strip geometry**: 2D lattice with open (free) boundary condition in both directions.
- **Cylindrical geometry**: 2D lattice with open (free) boundary condition in x-direction and periodic boundary condition in y-direction.
- **Torus geometry**: 2D lattice with periodic boundary condition in both directions.

Figure 2.2, shows these different geometries of the setup and chiral edge currents on them. Note that the geometry of the sample in real space has nothing to do with topology of the material. The reason behind the underlying topology of the material is the large contribution from the spin-orbit coupling of atoms. Hence, non-trivial topology of the material is the property of Bulk Hamiltonian and hence it does not depend on the geometry of the setup in real space. However, a particular geometry decides the nature of the setup boundaries and hence edge current pattern.

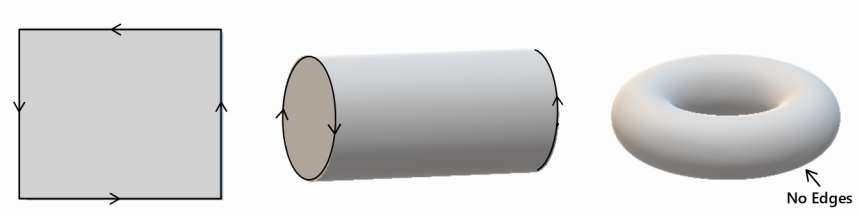

Figure 2.2: Various possible geometry of Chern insulator and the pattern of chiral edge currents on them

2.3 Band structure of Chern insulator

Band structure of spinless BHZ model can be obtained by squaring the momentum space Hamiltonian given in eq. (2.3). Squaring the Hamiltonian, we get the following equation:

$$\epsilon(k_x, k_y) = \pm\sqrt{\sin^2(k_x) + \sin^2(k_y) + (\mu_w^2 + \cos^2(k_x) + \cos^2(k_y))^2} \tag{2.7}$$

Here, k_x and k_y are good quantum numbers which can be used to label states. This is possible here because we have assumed an infinite lattice having translational invariance in both x and y direction. Such lattices don't have edges. In order to talk about edge states originating from the non-trivial topology of bulk band, we need to have open boundary condition in atleast one direction.

Let there be N_y no. of sites in $y-$ direction and infinite sites in $x-$direction. So, using open boundary condition in $y-$direction, it can be shown that $k_y = \frac{n\pi}{N_y+1}$, $n = 1, 2, 3, \cdots, N_y$. This will give $2 \times N_y$ no. of bands if we plot $\epsilon(k_x)$ for each k_y values. Following figure shows band diagram for $N_y = 10$:

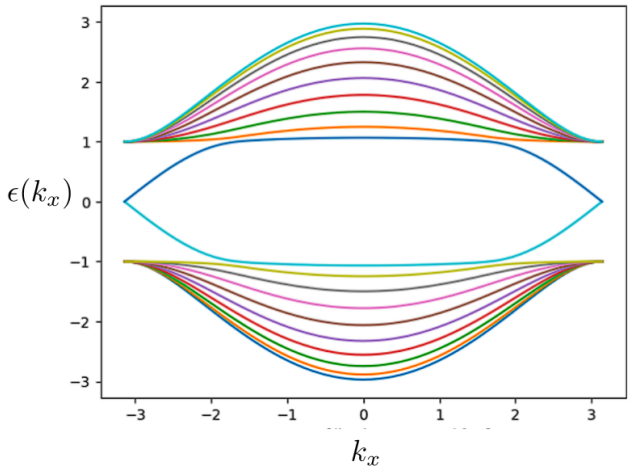

Figure 2.3: Band diagram for spinless BHZ model ($\mu_w = 1,\ N_y = 10$) with open boundary in $y-$direction.

Note that the band gap of SBHZ model lies between $-\mu_w$ to μ_w. We would keep $\mu_w = 1$ for the most part in this report. Since μ_w lies in the non-trivial regime ($-2 < \mu_w < 2$),we can clearly see the presence of edge states in the band gap (-1 to 1).

Chapter 3

Theoretical tools and the open system setup

In this chapter, we will discuss the NEGF formalism, the framework that help us to precisely frame the question of conductance quantization in an open system setup. We discuss the main results of NEGF and describe the finite strip geometry setup of Chern insulator connected to metallic leads. Later, we discuss the single particle Hamiltonian and self energy for 2D reservoirs, two main quantities in the expression of conductance. At the end, we discuss transfer matrix, a crucial tool which help us to analytically go beyond the formal expression of conductance.

3.1 Non-Equilibrium Green's Function (NEGF) formalism

Non-equilibrium Green's function is a formalism that provides a microscopic theory for Quantum Transport. It is a very general tool which can include the effects of various kinds of interaction (electron-electron, electron-phonon, etc) and disorders. Another key feature of this tool is its exact treatment of the effects of infinitely extended reservoirs. Hence, it is also a widely used tool to do direct numerics for tight-binding models. For the purpose of this report, we would be dealing mostly with tight-binding models with non-interacting

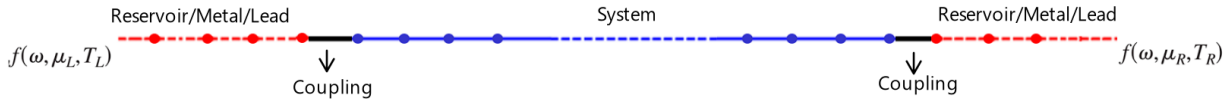

Figure 3.1: 1D example of a system connected connected to metallic leads

fermions for which the results of NEGF can be derived just by using Heisenberg equation of motion for bath and system operators [10].

The kind of setup we are interesting in, is that of a system (conductor or a Chern insulator) connected to metallic leads at its left and right ends (see fig. 3.1). The leads (both left and right) are actually semi-infinite reservoirs thermalized at different temperatures (T_L and T_R) and chemical potential (μ_L and μ_R). After certain time, the system connected to reservoirs reaches to a **Non-Equilibrium Steady State (NESS)**. We are interested in obtaining the NESS Current and conductance. We will start by writing the Hamiltonian for the total system.

Consider the following Hamiltonian of the full system:

$$H = \sum_{rs} H_{rs} c_r^\dagger c_s = H_W + H_L + H_R + V_L + V_R, \tag{3.1}$$

where

$$H_W = \sum_{lm} H^W_{lm} c_l^\dagger c_m, \qquad \text{(System's Hamiltonian)} \tag{3.2}$$

$$H_L = \sum_{\alpha\beta} H^L_{\alpha\beta} c_\alpha^\dagger c_\beta, \;\; H_R = \sum_{\alpha'\beta'} H^R_{\alpha'\beta'} c_{\alpha'}^\dagger c_{\beta'} \qquad \text{(Reservoir's Hamiltonian)} \tag{3.3}$$

$$V_L = \sum_{l\alpha} (V^L_{l\alpha} c_l^\dagger c_\alpha + V^{L\dagger}_{\alpha l} c_\alpha^\dagger c_l), \;\; V_R = \sum_{l\alpha'} (V^R_{l\alpha'} c_l^\dagger c_{\alpha'} + V^{R\dagger}_{\alpha' l} c_{\alpha'}^\dagger c_l), \qquad \text{(Coupling Hamiltonian)} \tag{3.4}$$

where $c_r^\dagger, c_r$ are fermionic creation and annihilation operators. Subscript W, L and R on Hamiltonian denotes wire, left and right respectively. A simple 1D example for a system connected to reservoirs is shown in figure 3.1.

Note that, all the terms in eq. 3.1 only assume quadratic nature (in terms of annihilation and creation operators). Except this, the nature of the hoppings could be arbitrary. Hence, the results mentioned here can be directly applied to our setup, Spinless BHZ connected to metallic leads, whose total Hamiltonian

have the quadratic nature.

Since, the total hamiltonian (of system + reservoir) is Hermitian, the operators will evolve according to Heisenberg equation of motion.

We want to obtain an expression for steady state current which can be defined as follows using the continuity equation.

$$J = \sum_{m\alpha} 2\,\mathrm{Im}\left(V^L_{m\alpha}\,\langle c^\dagger_m(t) c_\alpha(t)\rangle\right) \tag{3.5}$$

Using Fourier transform and Heisenberg equation of motion for bath and system operator, we can obtain the following expression [11]:

$$\boxed{J = 2\pi \int_{-\infty}^{\infty} d\omega\, \mathrm{Tr}(\Gamma_L \mathcal{G}^+ \Gamma_R \mathcal{G}^-)\,(f(\omega,\mu_L,T_L) - f(\omega,\mu_R,T_R))} \tag{3.6}$$

Before going into the details of the new notations appearing the above equation, let us see how the expression for the Conductance looks like.

Conductance for the system at the left junction (between system and reservoir) can be defined as follows:

$$G_2 = \frac{\partial J}{\partial \mu_L} \tag{3.7}$$

We use subscript on G_2 to emphasize that it is two-terminal conductance (to distinguish it from Hall conductance in 2D systems). Since we would be always working at 0K, Fermi distribution is given by a step function $\Theta(\omega - \mu_{L/R})$ and hence, taking the derivative inside the integral gives a delta-function leading to the following expression for Conductance:

$$\boxed{G_2(\omega) = \mathrm{Tr}(\Gamma_L(\omega)\mathcal{G}^+(\omega)\Gamma_R(\omega)\mathcal{G}^-(\omega))} \tag{3.8}$$

Now, we can summarize the useful results of the NEGF formalism which will be very frequently used in later chapters.

$\mathcal{G}^+(\omega)$ represents the effective Green's function of the system defined as:

$$\boxed{\mathcal{G}^+(\omega) = \frac{1}{\omega - H^W - \Sigma^+_L(\omega) - \Sigma^+_R(\omega)}} \tag{3.9}$$

where $\Sigma^{+}_{L,R}$ are self-energy terms coming due to the presence of left and right semi-infinite reservoirs. They can be written in terms of the isolated reservoir Green's functions $g^{+}_{L,R}(\omega)$ and the coupling matrices $V^{L,R}$ as follows [11]:

$$\boxed{\Sigma^{+}_{L}(\omega) = V^{L} g^{+}_{L}(\omega) V^{L\dagger}, \quad \Sigma^{+}_{R}(\omega) = V^{R} g^{+}_{R}(\omega) V^{R\dagger}} \tag{3.10}$$

Γ_L and Γ_R are the imaginary part of the self-energies:

$$\boxed{\Gamma_L(\omega) = \frac{1}{2\pi i}(\Sigma^{-}_{L} - \Sigma^{+}_{L}), \quad \Gamma_R(\omega) = \frac{1}{2\pi i}(\Sigma^{-}_{R} - \Sigma^{+}_{R})} \tag{3.11}$$

3.2 Chern insulator connected to metallic leads

We are interested in analytically understanding the quantization of two-terminal conductance observed in the quantum transport experiments [12] and numerical simulations [13] of Chern Insulator connected to metallic leads setup. We consider a finite strip geometry setup of Spinless BHZ connected to metallic leads as shown in figure 3.2. The Hamiltonian for the

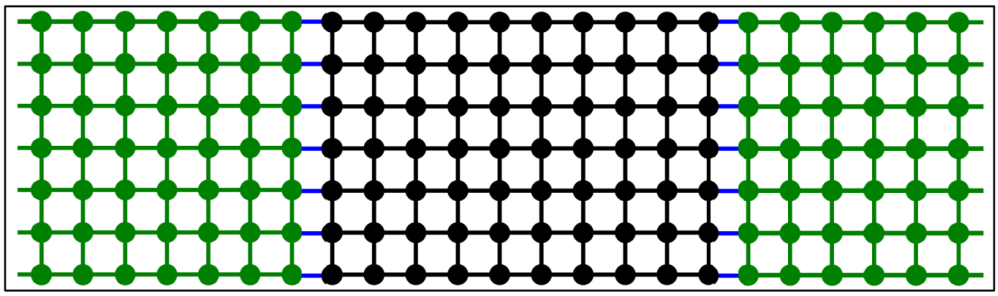

Figure 3.2: A finite strip geometry setup of Chern insulator connected to metallic leads. Black hopping- Chern insulator, green hopping- reservoir, blue hopping- coupling

total system is given by [13]:

,

$$H = H_W + H_L + H_R + H_{WL} + H_{WR} \tag{3.12}$$

where H_W represents the Spinless BHZ Hamiltonian given by,

$$\begin{aligned} H_W = & \sum_{x=1}^{N_x}\sum_{y=1}^{N_y}\mu_w\Psi^\dagger(x,y)\sigma_x\Psi(x,y) \\ & + \sum_{x=1}^{N_x}\sum_{y=1}^{N_y-1}\left[\Psi^\dagger(x,y)\frac{1}{2}(\sigma_x - i\sigma_z)\Psi(x,y+1) + h.c.\right] \\ & + \sum_{x=1}^{N_x-1}\sum_{y=1}^{N_y}\left[\Psi^\dagger(x,y)\frac{1}{2}(\sigma_x - i\sigma_y)\Psi(x+1,y) + h.c.\right] \end{aligned} \tag{3.13}$$

Here, $\Psi(x,y) = \begin{pmatrix}\psi_1(x,y) & \psi_2(x,y)\end{pmatrix}^T$ because of the presence of 2 internal degrees of freedom at each site.

The model for Reservoir taken here is a semi-infnite 2D nearest neighbour tight binding lattice (Each site has 2 internal degrees of freedom) with the following Hamiltonian. $\mathbb{I}_2$ will represent 2×2 identity matrix.

$$H_L = \sum_{x=-\infty}^{0}\sum_{y=1}^{N_y}\left[\Psi^\dagger(x,y)(\eta_b\mathbb{I}_2)\Psi(x+1,y) + h.c.\right] + \sum_{x=-\infty}^{0}\sum_{y=1}^{N_y}\left[\Psi^\dagger(x,y)(\tilde{\eta_b}\mathbb{I}_2)\Psi(x,y+1)h.c.\right] \tag{3.14}$$

$$H_R = \sum_{x=N_x+1}^{\infty}\sum_{y=1}^{N_y}\left[\Psi^\dagger(x,y)(\eta_b\mathbb{I}_2)\Psi(x+1,y) + h.c.\right] + \sum_{x=N_x+1}^{\infty}\sum_{y=1}^{N_y}\left[\Psi^\dagger(x,y)(\tilde{\eta_b}\mathbb{I}_2)\Psi(x,y+1) + h.c.\right] \tag{3.15}$$

System and reservoir are coupled by adding horizontal bonds between them using the following terms.

$$H_{WL} = \sum_{y=1}^{N_y}\left[\Psi^\dagger(-1,\ y)(\eta_c\mathbb{I}_2)\Psi(0,\ y+1) + h.c.\right] \tag{3.16}$$

$$H_{WR} = \sum_{y=1}^{N_y}\left[\Psi^\dagger(N_x,\ y)(\eta_c\mathbb{I}_2)\Psi(N_x+1,\ y+1) + h.c.\right] \tag{3.17}$$

3.3 Single particle Hamiltonian and self energy due to reservoirs

The expression for zero temperature conductance(eq. (3.8)) tells us that the only two ingredient included in it is the Hamiltonian and self energy due to reservoirs. So, here we will understand some details of the Hamiltonian and the self energy due to reservoirs.

From the previous section, we can see that the Hamiltonian of the entire setup is quadratic in nature because we would be dealing only with non-interacting fermions. As a result, we can work with the single particle Hamiltonians (which can be thought as a matrix of dimension equivalent to the number of sites in system) for each of the components. The summations in the eq. (3.13) can be written in a matrix form if we define a column vector Ψ using annhilation operators $\Psi(x, y)$ as follows:

$$\Psi = (\Psi(1,1), \Psi(2,1), \cdots, \Psi(N_x,1), \Psi(1,2), \Psi(2,2) \cdots \Psi(N_x,2) \cdots \Psi(1,N_y), \cdots \Psi(N_x,N_y))^T$$

Hence, the SBHZ Hamiltonian in strip geometry and written as

$$H_W = \Psi^\dagger H_{SBHZ} \Psi \tag{3.18}$$

where,

$$H_{SBHZ} = \begin{pmatrix} H_0 & H_1 & 0 & 0 & \cdots & 0 & 0 \\ {H_1}^\dagger & H_0 & H_1 & 0 & \cdots & 0 & 0 \\ 0 & {H_1}^\dagger & H_0 & H_1 & \cdots & 0 & 0 \\ 0 & 0 & {H_1}^\dagger & H_0 & \ddots & \vdots & \vdots \\ \vdots & \vdots & \vdots & \ddots & \ddots & H_1 & 0 \\ \vdots & \vdots & \vdots & \cdots & {H_1}^\dagger & H_0 & H_1 \\ 0 & 0 & 0 & \cdots & 0 & {H_1}^\dagger & H_0 \end{pmatrix} \tag{3.19}$$

H_{SBHZ} is a square matrix of order $2 \times N_x \times N_y$ (2 factor because each site has 2 internal degrees of freedom). Note that H_0 and H_1 in the above expression represents block matrices

of order $2 \times N_x$. H_0 represents the hopping between sites at fixed x and is given by:

$$H_0 = \begin{pmatrix} V & A & 0 & 0 & \cdots & 0 & 0 \\ A^\dagger & V & A & 0 & \cdots & 0 & 0 \\ 0 & A^\dagger & V & A & \cdots & 0 & 0 \\ 0 & 0 & A^\dagger & V & \ddots & \vdots & \vdots \\ \vdots & \vdots & \vdots & \ddots & \ddots & A & 0 \\ \vdots & \vdots & \vdots & \cdots & A^\dagger & V & A \\ 0 & 0 & 0 & \cdots & 0 & A^\dagger & V \end{pmatrix} \tag{3.20}$$

where V represents the site potential matrix (2×2) at each site defined by $\mu_w \times \sigma_z$ and $A = \frac{\sigma_z + i\sigma_y}{2}$ represents hopping matrix in x-direction (see eq.(3.13)).

H_1 represents hopping between $x = i$ and $x = i + 1$ layers defined as:

$$H_1 = \begin{pmatrix} B & 0 & 0 & 0 & \cdots & 0 & 0 \\ 0 & B & 0 & 0 & \cdots & 0 & 0 \\ 0 & 0 & B & 0 & \cdots & 0 & 0 \\ 0 & 0 & 0 & B & \ddots & \vdots & \vdots \\ \vdots & \vdots & \vdots & \ddots & \ddots & 0 & 0 \\ \vdots & \vdots & \vdots & \cdots & 0 & B & 0 \\ 0 & 0 & 0 & \cdots & 0 & 0 & B \end{pmatrix} \tag{3.21}$$

where, $B = \frac{\sigma_y + i\sigma_z}{2}$ is hopping matrix in y-direction (see eq. 3.13).

The single particle Hamiltonian for the metallic leads also have the same form as given in eq. 3.19 where V, A, B are replaced by $\mu_w \mathbb{I}_2$, $\eta_b \mathbb{I}_2$ and $\eta_b \mathbb{I}_2$ respectively.

Self energy due to reservoirs

Self energy $\Sigma_{L/R}$ appears in the system's effective green's function:

$$\mathcal{G}^+ = \frac{1}{\omega - H_W - \Sigma_L(\omega) - \Sigma_R(\omega)} \tag{3.22}$$

As a result, coupling two reservoirs to the system essentially adds two terms (Σ_L and Σ_R) in the Hamiltonian. They are defined by:

$$\Sigma_L = V_L^\dagger g_L^+(\omega) V_L \quad , \quad \Sigma_R = V_R^\dagger g_R^+(\omega) V_R \tag{3.23}$$

It can be shown that the self energy term for 2D reservoir is given by [14] :

$$\Sigma = U \Sigma_D U^\dagger \tag{3.24}$$

$$\text{where, } \Sigma_D[k,k] = \begin{cases} \frac{\eta_c^2}{\eta_b}\left[\alpha_k - i\sqrt{1-\alpha_k^2}\right], & |\alpha_k| < 1, \\ \frac{\eta_c^2}{\eta_b}\left[\alpha_k - \sqrt{\alpha_k^2 - 1}\right], & \alpha_k > 1, \\ \frac{\eta_c^2}{\eta_b}\left[\alpha_k + \sqrt{\alpha_k^2 - 1}\right], & \alpha_k < -1, \end{cases} \tag{3.25}$$

with $\alpha_k = \frac{\omega - \lambda_k}{\eta_b}$. Here, $\lambda_k = -2t\cos(k)$ and U is the unitary matrix that diagonalizes the H_0 Hamiltonian. Hence, from the matrix form of self energy, it is clear that they just add to the boundary blocks of the Hamiltonian. **Physically, it means that the reservoirs essentially add complex site potentials and complex long range hoppings to the $x = 1$ and $x = N_x$ layers of the 2D Chern insulator lattice.**

3.4 Transfer matrix

Transfer matrix is an analytic tool that helps to connect wavefunctions at different sites by exploiting the tri-diagonal structure of the tight-binding Hamiltonian. It can also be used to connect matrix elements of Green's function which is the key quantity to calculate two terminal conductance (G_2).

To see this more clearly, consider a 1-D nearest neighbour tight binding system with N number of sites connected to 1-D semi-infinite metallic leads (which are also modelled by 1D nearest neighbour tight-binding Hamiltonian) (as shown in fig.3.1):

$$G_2(\omega) = \mathrm{Tr}(\Gamma_L(\omega)\mathcal{G}^+(\omega)\Gamma_R(\omega)\mathcal{G}^-(\omega)) \tag{3.26}$$

Here, let Γ_L and Γ_R be the imaginary part of the self energy of wide band reservoirs (for more details about wide band limit, see section 4.3):

$$\Gamma_L = \begin{pmatrix} \gamma & 0 & 0 & \cdots & 0 & 0 & 0 \\ 0 & 0 & 0 & \cdots & 0 & 0 & 0 \\ 0 & 0 & 0 & \cdots & 0 & 0 & 0 \\ \vdots & \vdots & \vdots & \ddots & \vdots & \vdots & \vdots \\ 0 & 0 & 0 & \cdots & 0 & 0 & 0 \\ 0 & 0 & 0 & \cdots & 0 & 0 & 0 \\ 0 & 0 & 0 & \cdots & 0 & 0 & 0 \end{pmatrix} \text{ and } \Gamma_R = \begin{pmatrix} 0 & 0 & 0 & \cdots & 0 & 0 & 0 \\ 0 & 0 & 0 & \cdots & 0 & 0 & 0 \\ 0 & 0 & 0 & \cdots & 0 & 0 & 0 \\ \vdots & \vdots & \vdots & \ddots & \vdots & \vdots & \vdots \\ 0 & 0 & 0 & \cdots & 0 & 0 & 0 \\ 0 & 0 & 0 & \cdots & 0 & 0 & 0 \\ 0 & 0 & 0 & \cdots & 0 & 0 & \gamma \end{pmatrix} \tag{3.27}$$

where $\gamma = \frac{\eta_c^2}{\eta_b}$. Using this, eq. (3.26) simplifies to

$$G_2 = \gamma^2 \mathrm{Tr}(\mathcal{G}_{1N}^{+} \mathcal{G}_{1N}^{-}). \tag{3.28}$$

Hence, one essentially needs $\mathcal{G}_{1N}$ element of green's function to obtain conductance. This might seem a very non-trivial problem as we need to invert the effective Green's function (a $N_x \times N_x$ matrix). But, such difficulty can be easily bypassed by exploiting the tri-diagonal structure of the system hamiltonian.

Effective Green's function satisfies the following equation:

$$(\omega - H_W - \Sigma_L - \Sigma_R)\mathcal{G}^{+}(\omega) = \mathbb{I} \tag{3.29}$$

$$\begin{pmatrix} \omega - \mu_w - \Sigma & -t & 0 & 0 & \cdots & 0 & 0 \\ -t & \omega - \mu_w & -t & 0 & \cdots & 0 & 0 \\ 0 & -t & \omega - \mu_w & -t & \cdots & 0 & 0 \\ \vdots & \vdots & -t & \omega - \mu_w & \ddots & \vdots & \vdots \\ \vdots & \vdots & \vdots & \ddots & \ddots & -t & 0 \\ \vdots & \vdots & \vdots & \cdots & -t & \omega - \mu_w & -t \\ 0 & 0 & 0 & \cdots & 0 & -t & \omega - \mu_w - \Sigma \end{pmatrix} \begin{pmatrix} \mathcal{G}_{11} & \cdots \\ \mathcal{G}_{21} & \cdots \\ \mathcal{G}_{31} & \cdots \\ \vdots & \cdots \\ \vdots & \cdots \\ \mathcal{G}_{N_x-1,1} & \cdots \\ \mathcal{G}_{N_x 1} & \cdots \end{pmatrix} = \begin{pmatrix} 1 & 0 & \cdots \\ 0 & 1 & \cdots \\ 0 & 0 & \cdots \\ \vdots & \vdots & \cdots \\ \vdots & \vdots & \cdots \\ 0 & 0 & \cdots \\ 0 & 0 & \cdots \end{pmatrix} \tag{3.30}$$

First row of RHS and LHS give us the following set of equations:

$$(\omega - \mu_w - \gamma)\mathcal{G}_{11} - t\mathcal{G}_{12} = 1 \tag{3.31}$$

$$-t\mathcal{G}_{1,x-1} + (\omega - \mu_w)\mathcal{G}_{1,x} - t\mathcal{G}_{1,x+1} = 0 \quad (2 \leq x \leq N) \tag{3.32}$$

$$-t\mathcal{G}_{1,N-1} + (\omega - \mu_w - \gamma)\mathcal{G}_{1N} = 0 \tag{3.33}$$

These equations can be rewritten in matrix form as follows:

$$\begin{pmatrix} 1 \\ \mathcal{G}_{11} \end{pmatrix} = \begin{pmatrix} \omega - \mu_w - \gamma & -t \\ 1 & 0 \end{pmatrix} \begin{pmatrix} \mathcal{G}_{11} \\ \mathcal{G}_{12} \end{pmatrix} \tag{3.34}$$

$$\begin{pmatrix} \mathcal{G}_{1,x-1} \\ \mathcal{G}_{1,x} \end{pmatrix} = \begin{pmatrix} \frac{\omega-\mu_w}{t} & -1 \\ 1 & 0 \end{pmatrix} \begin{pmatrix} \mathcal{G}_{1,x} \\ \mathcal{G}_{1,x+1} \end{pmatrix} \qquad (2 \leq x \leq N) \tag{3.35}$$

$$\begin{pmatrix} \mathcal{G}_{1,N-1} \\ \mathcal{G}_{1N} \end{pmatrix} = \begin{pmatrix} \frac{\omega-\mu_w-\Sigma}{t} & 0 \\ 1 & 0 \end{pmatrix} \begin{pmatrix} \mathcal{G}_{1N} \\ 0 \end{pmatrix} \tag{3.36}$$

We label the matrices as follows:

$$\Omega_L = \begin{pmatrix} \omega - \mu_w - \gamma & -t \\ 1 & 0 \end{pmatrix} \quad \Omega = \begin{pmatrix} \frac{\omega-\mu_w}{t} & -1 \\ 1 & 0 \end{pmatrix} \quad \Omega_R = \begin{pmatrix} \frac{\omega-\mu_w-\Sigma}{t} & 0 \\ 1 & 0 \end{pmatrix} \tag{3.37}$$

Using these matrices, we can write the following equation:

$$\begin{pmatrix} 1 \\ \mathcal{G}_{11} \end{pmatrix} = \Omega_L \Omega^{(N-1)} \Omega_R \begin{pmatrix} \mathcal{G}_{1N} \\ 0 \end{pmatrix} \tag{3.38}$$

Let $\tilde{\Omega} = \Omega_L \Omega^{N-1} \Omega_R$, then

$$\begin{pmatrix} 1 \\ \mathcal{G}_{11} \end{pmatrix} = \begin{pmatrix} \tilde{\Omega}_{11} & \tilde{\Omega}_{12} \\ \tilde{\Omega}_{21} & \tilde{\Omega}_{22} \end{pmatrix} \begin{pmatrix} \mathcal{G}_{1N} \\ 0 \end{pmatrix} \tag{3.39}$$

So,

$$\boxed{\mathcal{G}_{1N} = \tilde{\Omega}_{11}^{-1}} \tag{3.40}$$

Hence, $\mathcal{G}_{1N}$ element can be obtained using 1, 1 element of $\tilde{\Omega}$. Obtaining this matrix element is now very simple as one can use spectral decomposition of Ω and analytically obtain $\tilde{\Omega}$ which is a much simpler task than inverting a $N_x \times N_x$ matrix in eq. 3.30.

Part II

Results

Chapter 4

Strip geometry setup

In this chapter we discuss a finite strip geometry of the Spinless BHZ model—a 2D Chern insulator—coupled to metallic leads at 0K (ref. [13]). We start by presenting key plots reproduced from the ref. [13] and then present numerical results that reveal oscillatory features in the spectrum of the effective non-Hermitian Hamiltonian. Further, we analyze a modified setup where one reservoir is replaced by a Chern insulator, resulting in the disappearance of these oscillations. These findings indicate that the reservoir self-energy can be simplified using the wide band limit, as supported by additional numerical tests. At the end, we demonstrate that employing 1D reservoirs is insufficient for achieving quantized conductance in the thermodynamic limit, emphasizing the necessity of 2D reservoirs.

4.1 Oscillations in conductance and their signature in non-hermitian Hamiltonian

Considering the strip geometry setup for Chern insulator setup connected to metallic leads (as shown in fig. 3.2), we can obtain the behaviour of conductance using the formal NEGF expression for two terminal conductance, see eq.(3.8). We get the plot as shown in fig. 4.1 below for two-terminal conductance as we tweak the fermi-level (controlled by the chemical potential of the reservoir). This plot numerically verifies that the two-terminal conductance is indeed quantized in an open system setup when $\mu \in (-1, 1)$, i.e. Band gap of Chern

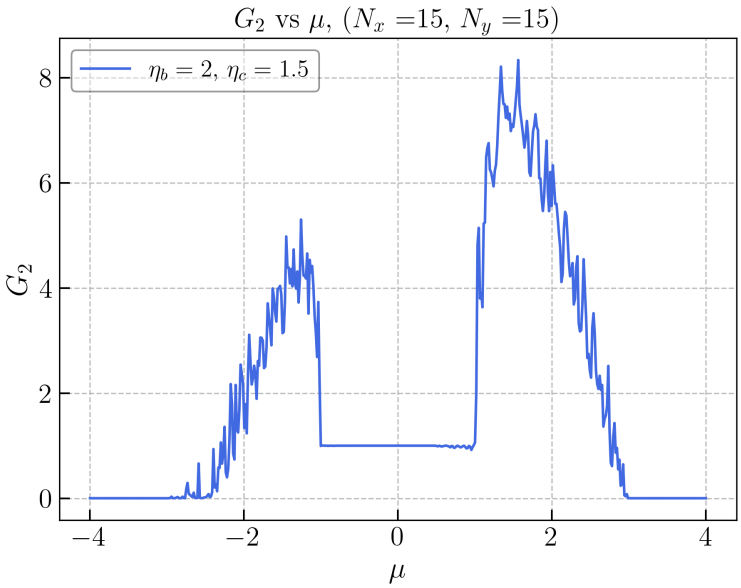

Figure 4.1: Two terminal conductance vs μ (parameters: $N_x = N_y = 15$, $\eta_c = 1.5, \eta_b = 2$)

insulator

Following are the two natural questions that arises in this setup:

- How does the quantization of conductance gets affected due to the details at the interface of Metal-Chern insulator junction ?

- How does the finite size of lattice affects the quantization?

These questions were studied numerically in reference [13]. We have reproduced their numerical result in figure 4.2. It can be seen that the plots have oscillating behaviour at small values of η_c (which models the coupling between system and metallic lead) and N_y. As one increases η_c or N_y (keeping other parameters fixed), conductance starts to tend 1. However, reference [13] does not explore the underlying cause of the oscillating behavior. In the following section, we present a numerical result that provides some insights into this oscillating nature of conductance.

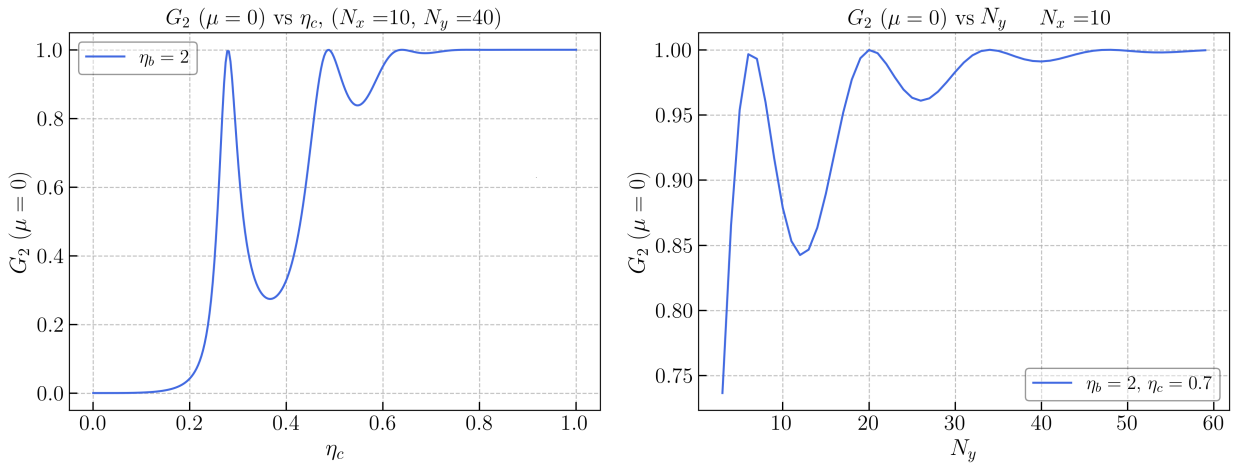

Figure 4.2: Oscillation in conductance with increase in η_c and N_y

4.1.1 Explaining the oscillating conductance

The oscillations observed in fig. 4.2 are very similar to the one observed in the textbook problem of scattering through finite 1D potential well (see fig. 4.3). There we see that, perfect transmission ($T = 1$) occurs if the scattering particle have the energy equal to the eigenvalues of the infinite 1D well problem. Understanding this simple textbook problem

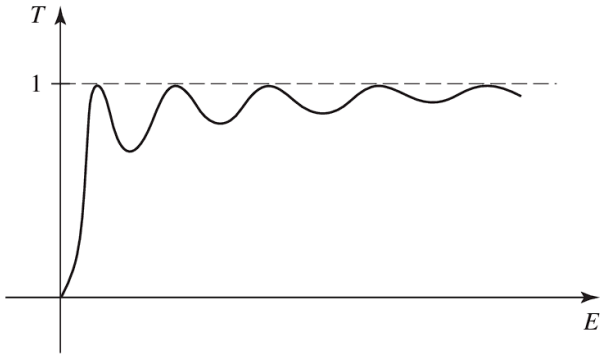

Figure 4.3: Transmission amplitude for a particle (with energy E) scattering through a finite potential well [15]

suggests that the conductance oscillations are linked to the system's eigenvalues. To explore this further, we examine the spectrum[1] of the isolated Chern Insulator model (Spinless BHZ). As evident from the spectrum (fig.4.4), the model exhibits eigenvalues within the band gap

[1]spectrum is obtained by numerically diagonalizing the single particle Hamiltonian (eq. 3.19)

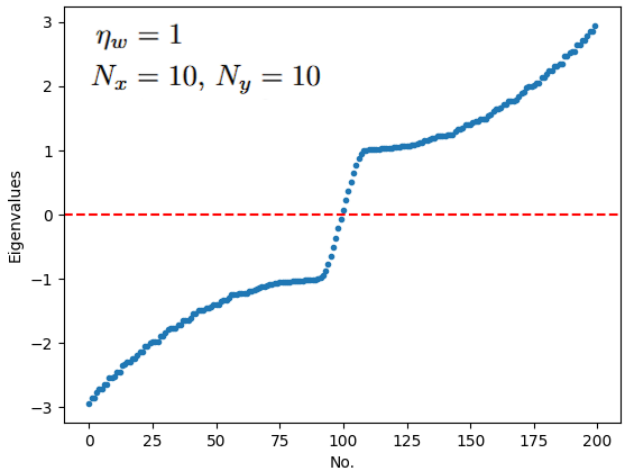

Figure 4.4: Eigenvalues of an isolated SBHZ model (Red line represents Fermi level ($\mu = 0$))

(between -1 and 1), which correspond to the edge states. When an eigenvalue of the isolated Chern Insulator Hamiltonian (for a single electron) is close to or coincides with the chemical potential μ, the system supports the conduction of electrons injected from the reservoir at that energy. Just to emphasize, in this section, μ should be thought of as the energy of the electron injected into the Chern Insulator.

Properties of reservoir and how it couples to system also affects the spectrum of the system. These effects are taken into account by self energy terms (defined in section 3.3) present in the effective Hamiltonian of the system:

$$H_{\text{eff}} = H_{\text{chern}} + \Sigma_L(\mu) + \Sigma_R(\mu) \tag{4.1}$$

In the 1D scattering problem for finite well, perfect transmission is achieved when the particle's energy matches the eigenvalues of the infinite well. In contrast, for the Chern Insulator setup, the Fermi level (or reservoir chemical potential) is held fixed. However, the coupling to the reservoirs affects the eigenvalues of the Chern Insulator through the self-energy terms incorporated into H_{eff}. By numerically diagonalizing H_{eff} , we observe that the energy of the edge states shifts as we tweak η_c or N_y.

In the following subsections, we will fix the fermi level at $\mu = 0$ and see how the energy of the edge state closest to $\mu = 0$ oscillates as we increase coupling (η_c) or N_y.

$G(\mu = 0)$ **Vs** η_c

Plotting the eigenvalue closest to $\mu = 0$ as a function of the coupling parameter η_c reveals an oscillatory behavior. These oscillations indicate that perfect transmission is observed only when an edge state is at the Fermi level. As the coupling is tuned, the edge state energies oscillate—moving closer to and further from the Fermi level—thereby producing the observed conductance oscillations.

The spectrum for the effective Hamiltonian $(H_{\text{chern}} + \Sigma_R + \Sigma_L)$[2] depends on the coupling because of the self energy terms (Σ_L and Σ_R) in the Hamiltonian. Hence, as we vary η_c, spectrum of non-hermitian Hamiltonian will also vary. Figure 4.5 b) is the plot for showing the oscillation in eigenvalue closest to fermi-level as we increase coupling. More precisely, it is the plot$\{|Re(\lambda)|\}_{min}$ Vs η_c (where $\{|Re(\lambda)|\}_{min}$ represents the smallest absolute value of real part of an eigenvalue out of all eigenvalues of the effective non Hermitian Hamiltonian for a fixed η_c).
Using fig. 4.5 b), we can explain the most crucial feature of the fig. 4.5 a), that is oscillations in conductance. So essentially, as we increase η_c, eigenvalue closest to $E = 0$ also changes. For certain value of η_c there is an eigenvalue very close to $E = 0$ which supports the perfect transmission of electron through the system, leading to peaks in fig. 4.5 a). As a result, we can see that there is a good agreement between maxima and minima of fig. 4.5 a) to the minima and maxima of fig. 4.5 b).

$G(\mu = 0)$ **Vs** N_y

Fig. 4.6 has plots of very similar nature compared to fig. 4.5 and hence we can explain the oscillatory behaviour by similar arguments using the spectrum of the effective non-Hermitian Hamiltonian.
The value of N_y at which conductance's maxima and minima occurs in fig. 4.6 a), decently matches with minima and maxima of the 4.6 b) for the same reason explain in the previous part.

[2]Expressions for the self energy can be analytically obtained for infinite size bath (See Ref. [14], eq(9))

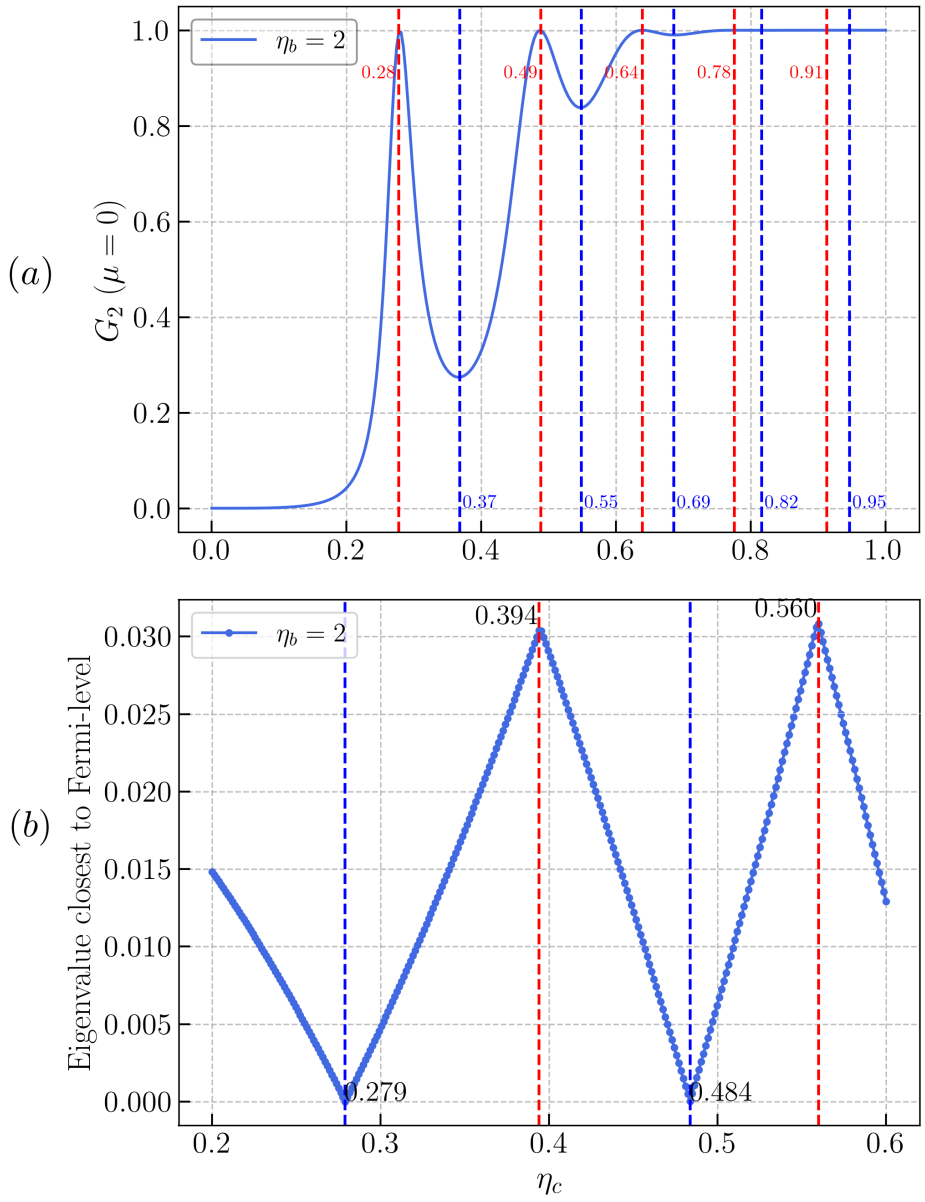

Figure 4.5: Comparision of a) oscillation in conductance and b) oscillation in the real part of eigenvalue (of $H_{\mathbf{eff}}$) closest to Fermi level as we increase coupling (η_c)

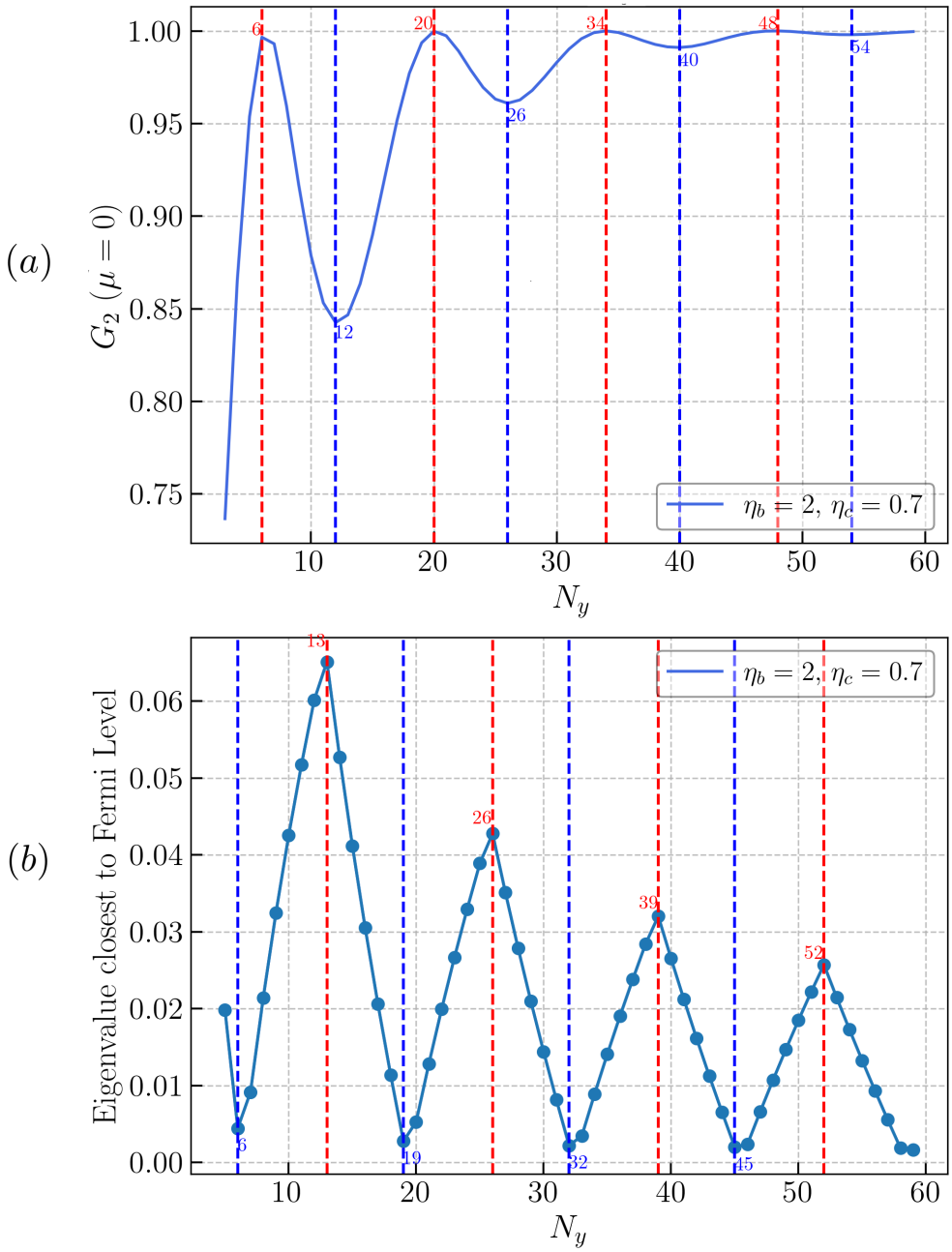

Figure 4.6: Comparision of a) oscillation in conductance and b) oscillation in the real part of eigenvalue (of $H_{\mathbf{eff}}$) closest to Fermi level as we increase N_y.

4.1.2 Summary

- Using the spectrum of the Non-hermitian Hamiltonian, $H_{\text{eff}} = H_W + \Sigma^+(\mu) + \Sigma^-(\mu)$, we showed that peaks and dips in SBHZ conductance plots ($G\ vs\ \eta_c$ and $G\ vs\ N_y$) is very well related to the peaks and dips of oscillation in the spectrum of the non-hermitian SBHZ Hamiltonian.

- It turns out that the closest eigenvalue to fermi level of non-hermitian SBHZ Hamiltonian, oscillates with η_c in the exact same way as the conductance of SBHZ model oscillates with η_c.

- Effect of self energy in Effective non-hermitian Hamiltonian is to essentially add complex site potential at the boundary of Chern Insulator. The real part of self energy shifts the energy of the edge states. As a result, increasing coupling strength (present in self energy) shifts the eigenvalues continuously. As soon as the value of an edge state hits the fermi level, there is perfect transmission of electron.

- Hence, numerics suggests that the quantization of conductance at some specific discrete values of η_c and N_y at finite lattice sizes is not so surprising and is independent of the problem of quantization of Conductance as one sees approaching it to 1 in the thermodynamic limit. Note, that the spectrum of non-Hermitian Hamiltonian still does not explains why at stronger coupling and larger N_y, two terminal conductance tends to 1.

4.2 Absence of oscillations - KWANT implementation

In order to further understand the origin behind oscillations, we considered a different setup where one of the metallic lead is replaced by Chern Insulator itself. The setup then looks as follows: Recall that the two key ingredients in the two terminal conductance expression is

Figure 4.7: Chern insulator (CI) setup with metallic leads on only one side

Chern insulator Hamiltonian and self energy of metallic leads. A formal expression for self energy of the metallic lead reservoir can be obtained analytically [14] which can be used for numerics. However obtaining self energy for Chern insulator reservoir is very difficult due to non-trivial block matrix structure of the single particle Hamiltonian (see eq. 3.19). As a result, the setup shown in fig. 4.7 cannot be implemented numerically in the usual way.

As a result, we use KWANT python package [16], a versatile and simple to use tool for quantum transport simulations. Using KWANT, it becomes much easier to implement the setup shown in fig. 4.7.

So what happens to oscillations in this new setup? It is a bit surprising that oscillations are no more there in G_2 vs η_c and G_2 vs N_y plots as shown in the fig. 4.8. These plots can be compared to plots for Chern insulator with two metallic lead reservoirs shown in fig. 4.2.

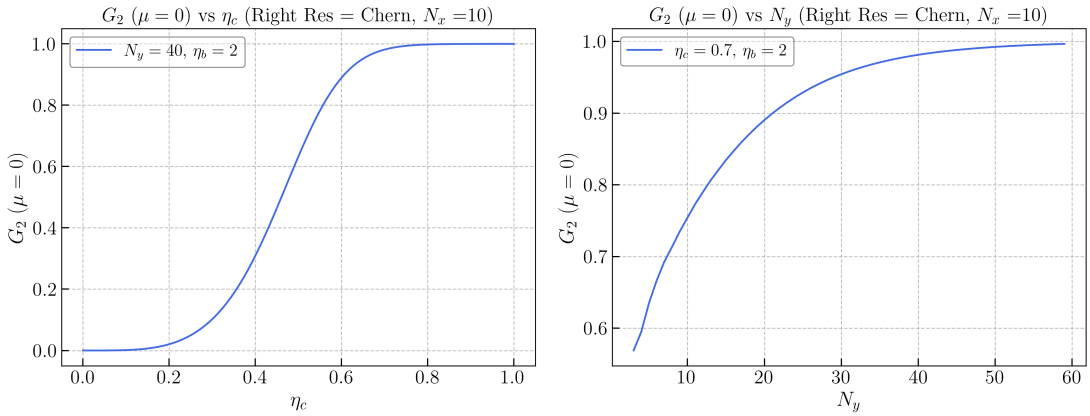

Figure 4.8: G_2 as a function of coupling and N_y when right reservoir is itself Chern insulator

4.2.1 A possible intuitive explanation for absence of oscillation

A possible intuitive explanation comes from looking at the current pattern at similar parameter values in Chern insulator setup at $\mu = 0$ as shown in fig. 4.9 . From this plot, it is clear that the electron essentially undergoes a 1D channel due to presence of edge state. In this edge state, we know that the electron would be travelling ballistically without scattering. So, the only region of setup that can affect the transmission of electron are the junctions at the two boundaries (left and right) of Chern insulator. We also know that the effect of reservoirs can be taken into account by adding self energy terms in the Hamiltonian leading to an effective Hamiltonian for the total system (given by eq. 4.1). A key effect of self energy terms is to add complex site-potentials at the boundary (left and right) sites of Chern insulator (this can be easily seen by explicitly evaluating the self energy matrices). Real part of self energy acts as a real site-potential whereas imaginary part of self energy act as a source/sink of particles. We would be only considering the effect of real part of self energy as the role of imaginary part is bit subtle and irrelevant for the explanation of oscillations. So, taking these things into account, fig. 4.10 depicts the potential that electron would be

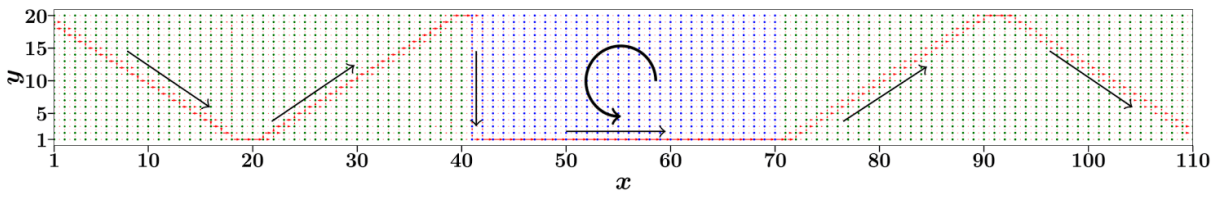

Figure 4.9: Current pattern in Metal-Chern insulator-Metal setup at $\mu = 0$. This figure is taken from ref. [13].

.

experiencing in the edge channel. The electron experiences a series of site potential on the left boundary. Note that this series of discrete site potential on lattice can be modelled by a rectangular barrier(and not a series of delta potential) in the continuum space. Since electron then travels on the bottom edge (see fig. 4.9), it only experiences a single site potential at the right boundary which can be modelled by a dirac delta potential in continuum space as shown in fig. 4.10 (right).

So the problem of obtaining conductance in Chern insulator setup is analogous to obtaining transmission probability of a quantum particle scattering through a potential shown in the above figure. This is a standard textbook problem [15] and such double barrier problems are well studied in literature [17] where the resonant tunelling phenomena occurs due to the wave

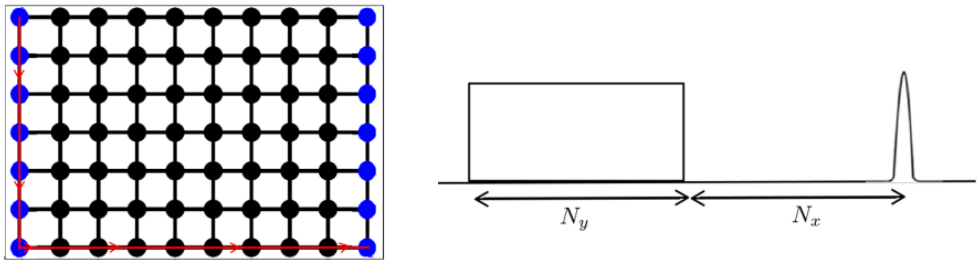

Figure 4.10: Left: Electron flowing at the edges is shown by red arrows. Blue dots represent complex site potential added by self energy terms in the effective Hamiltonian. Right: This diagram shows the schematic potential the electron would be experiencing inside edge channel due to presence of reservoirs.

nature of quantum particle. So, this oscillatory nature of conductance/transmission probablity (see fig. **??** and 4.3) is due to electron's wavefunction accumulating phase (leading to interference) as we tweak some parameter of the setup. So, replacing the right reservoir with Chern Insulator removes the barrier experienced by the electron at the junction on the right side of the setup. Hence, there are no two barrier between which successive reflections can happen for oscillation to occur. Hence, we don't see any oscillation when right reservoir is Chern insulator. This oscillation due to real part of self energy should also go away if we have only purely imaginary self energy. It turns out that this is indeed the case as we will see in the next section.

4.3 Simplification in the metallic lead model

From the analysis of the edge spectrum of H_{eff} and understanding the effect of real part of self energy on the spectrum, it seems that the real part of self energy is not relevant for the problem of quantization. This can be tested using a simplified setup shown in the figure below:

Instead of 2D metallic lead of width N_y, we have connected N_y no. of 1D metallic leads.

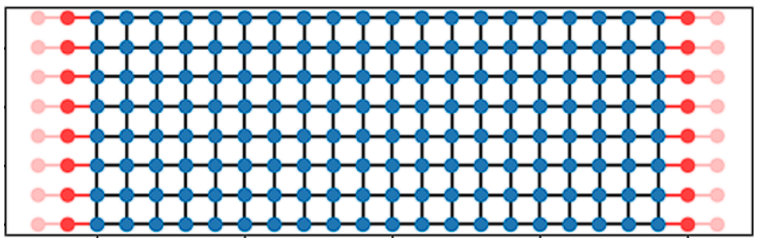

Figure 4.11: Chern insulator connected to 1D metallic leads

The self energy for each such 1D lead is given by [11],

$$\Sigma_{1D}(\mu) = \frac{{\eta_c}^2}{\eta_b}\left[\frac{\mu}{2\eta_b} - i\sqrt{1-\frac{\mu^2}{4\eta_b^2}}\right] \tag{4.2}$$

and hence, the self energy matrix in H_{eff} looks like

$$\Sigma = \begin{pmatrix} \Sigma_{1D} & 0 & 0 & \cdots & 0 & 0 & 0 \\ 0 & \Sigma_{1D} & 0 & \cdots & 0 & 0 & 0 \\ 0 & 0 & \Sigma_{1D} & \cdots & 0 & 0 & 0 \\ \vdots & \vdots & \vdots & \ddots & \vdots & \vdots & \vdots \\ 0 & 0 & 0 & \cdots & \Sigma_{1D} & 0 & 0 \\ 0 & 0 & 0 & \cdots & 0 & \Sigma_{1D} & 0 \\ 0 & 0 & 0 & \cdots & 0 & 0 & \Sigma_{1D} \end{pmatrix} \tag{4.3}$$

Taking the limit (called Wide Band (WB) limit), $\eta_b,\ \eta_c \to \infty$ with $\frac{\eta_c^2}{\eta_b} = \gamma = \text{constant}$, we get

$$\boxed{\Sigma_{1D} = \frac{-i\eta_c^2}{\eta_b}} \quad \text{(for wide band reservoir)} \tag{4.4}$$

Note that there is no real part of self energy. Real part was causing oscillation in conduc-

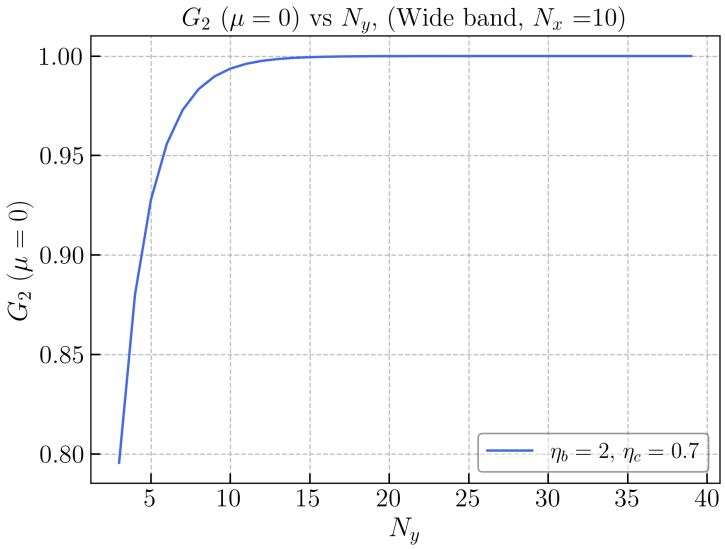

Figure 4.12: $G_2(\mu = 0)$ vs N_y plot for wide band reservoir

tance. Hence, we expect that the oscillation would go away if we use wide band reserovoir. This indeed turns out to be true. If we look at fig. 4.12, there is no oscillation present, leading to a simpler behaviour of conductance. So, the wide band reservoir simplifies the analytic expression for self energy and still captures the quantization feature of conductance. Following numerical plot shows $G_2(\mu)$ vs μ plot for setup with Wide Band reservoir:

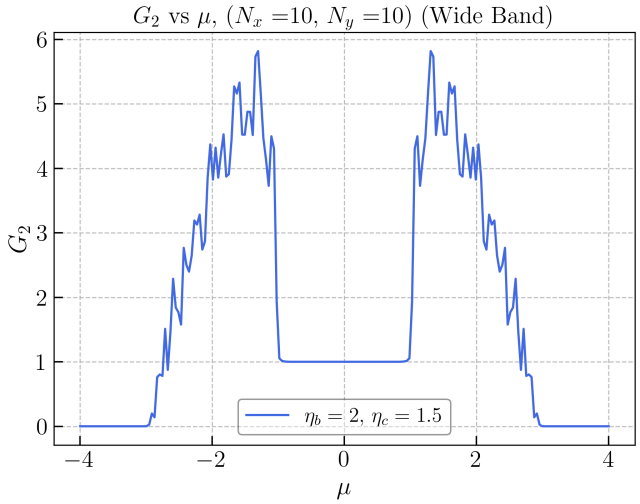

Figure 4.13: G_2 vs μ plot for wide band reservoir

4.4 Absence of quantization in an oversimplified setup

A further simplification that comes naturally in mind is the setup with just one 1D lead connected as shown in figure below:

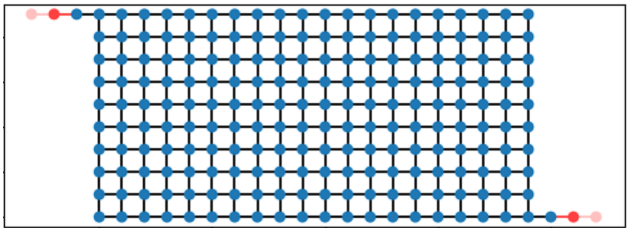

Figure 4.14: Chern insulator setup with one 1D reservoir connected

This setup could simplify analytic calculations because our 2D reservoir self energy simplifies to 1D reservoir self energy. But, does this setup still shows quantization? Numerically

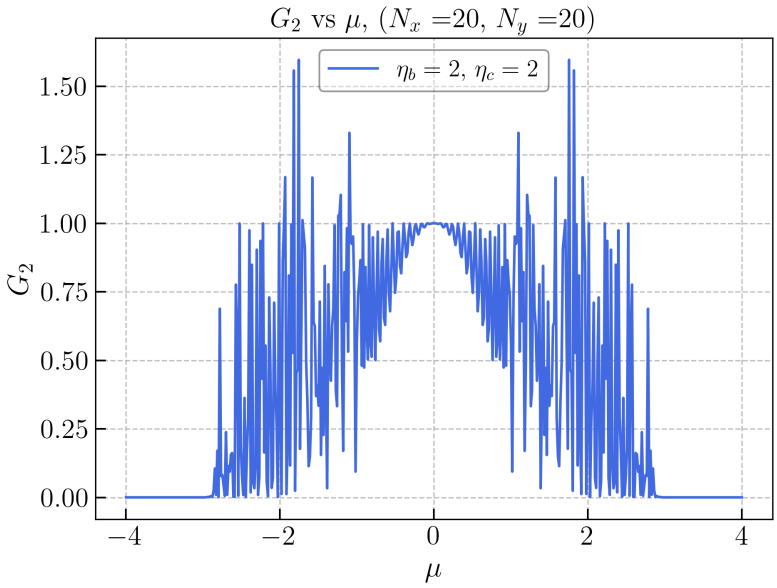

Figure 4.15: G_2 vs μ plot for setup with one 1D lead. (Parameters: $\eta_b = \eta_c = 2, N_x = N_y = 20$)

obtaining the conductance plot shows that 1D reservoirs are not sufficient to observe quantization as shown in figure 4.15.

This plot tells us that increasing N_y leads to quantization because the no. of injections increases in 2D reservoir setup (shown in fig.4.11) with N_y. However, the no. of injection is fixed (equal to one) in this case which leads to no effect of increasing lattize size on the conductance.

Chapter 5

Cylindrical geometry setup

In this chapter, we consider a cylindrical geometry for Chern insulator connected to metallic leads. Although this cylindrical setup differs from the typical strip-like geometries considered in experimental setups, it provides valuable analytic simplifications. In strip-like geometry, analytical calculations are cumbersome and do not yield neat expressions for two-terminal conductance that explain its quantization in the thermodynamic limit.

Motivated by Hatsugai [18], we adopt a cylindrical geometry to reduce a 2D transport problem to a 1D tranport problem. We start by defining the setup and showing that Fourier transforming the spinless BHZ model in one direction essentially gives a set of 1D SSH chains. Due to the lack of edges in x-direction in the cylindrical geometry, no current flow along the horizontal direction. Hence, we define a new quantity, calling it Hall conductance using the vertical current (see fig. 2.2 for current pattern in cylindrical geometry). Using matrix representation for Fourier-transform along y-direction, we show that the NEGF expression for Hall conductance simplifies due to cylindrical symmetry.

Since 2D Chern insulator essentially becomes a set of 1D SSH chains, one can use transfer matrix for SSH chain to further simplify the Hall conductance expression. In section 5.5, an explicit derivation of the transfer matrix for SSH chain is given. Using spectral decomposition of this transfer matrix, a simple expression of Hall conductance is derived in the thermodynamic limit ($N_x, N_y \to \infty$). This expression is essentially an integral over a coupling dependent integrand. Numerically, we show that this integral expression is independent of coupling which indicates that Hall conductance in an open system setup is indeed

quantized in the thermodynamic limit. We conclude this chapter by giving an analytic proof of quantization in the weak coupling limit.

5.1 Setup

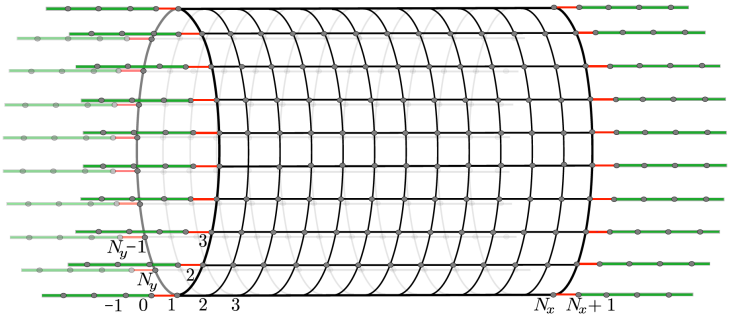

Figure 5.1: Metal-Chern insulator-Metal setup in Cylindrical geometry

The Hamiltonian for the SBHZ model [13] in cylindrical geometry is given by,

$$\begin{aligned} H_W = & \sum_{x=1}^{N_x}\sum_{y=1}^{N_y} \mu_w \Psi^\dagger(x,y)\sigma_x\Psi(x,y) \\ & + \sum_{x=1}^{N_x}\sum_{y=1}^{N_y}\left[\Psi^\dagger(x,y)\frac{1}{2}(\sigma_x - i\sigma_z)\Psi(x,y+1) + h.c.\right] \\ & + \sum_{x=1}^{N_x-1}\sum_{y=1}^{N_y}\left[\Psi^\dagger(x,y)\frac{1}{2}(\sigma_x - i\sigma_y)\Psi(x+1,y) + h.c.\right] \end{aligned} \tag{5.1}$$

with $\Psi(x,1) = \Psi(x,N_y+1)$. Note that $\Psi(x,y) = \begin{pmatrix}\psi_1(x,y) & \psi_2(x,y)\end{pmatrix}^T$ because of the 2 internal degrees of freedom at each site.

The model for Reservoir taken here is a 2D cylindrical nearest neighbour tight binding lattice (Each site has 2 internal degrees of freedom) with the following Hamiltonian. $\mathbb{I}_2$ will represent 2×2 identity matrix.

$$H_L = \sum_{x=-\infty}^{0} \sum_{y=1}^{N_y} \left[\Psi^\dagger(x,y)(\eta_b \mathbb{I}_2)\Psi(x+1,y) + h.c.\right] + \sum_{x=-\infty}^{0} \sum_{y=1}^{N_y} \left[\Psi^\dagger(x,y)(\tilde{\eta_b} \mathbb{I}_2)\Psi(x,y+1) h.c.\right] \tag{5.2}$$

$$H_R = \sum_{x=N_x+1}^{\infty} \sum_{y=1}^{N_y} \left[\Psi^\dagger(x,y)(\eta_b \mathbb{I}_2)\Psi(x+1,y) + h.c.\right] + \sum_{x=N_x+1}^{\infty} \sum_{y=1}^{N_y} \left[\Psi^\dagger(x,y)(\tilde{\eta_b} \mathbb{I}_2)\Psi(x,y+1) + h.c.\right] \tag{5.3}$$

System and reservoir are coupled by adding horizontal bonds between them using the following terms.

$$H_{LW} = \sum_{y=1}^{N_y} \left[\Psi^\dagger(-1,\ y)(\eta_c \mathbb{I}_2)\Psi(0,\ y+1) + h.c.\right] \tag{5.4}$$

$$H_{WR} = \sum_{y=1}^{N_y} \left[\Psi^\dagger(N_x,\ y)(\eta_c \mathbb{I}_2)\Psi(N_x+1,\ y+1) + h.c.\right] \tag{5.5}$$

Simplified Reservoir limit

In order to simplify our calculations, we will work with a simpler reservoir (in the wide band limit) which is the reservoir defined in Eq. (5.2) and (5.3) with the following conditions:

$$\tilde{\eta_b} = 0$$

$$\eta_b,\ \eta_c \to \infty \quad \text{with} \quad \frac{\eta_c^2}{\eta_b} = \gamma = \text{constant}$$

This reservoir essentially represents a set of 1D leads (as shown in Fig. 5.1) in the wide band limit. The advantage of using it is that, it simplifies the analysis of conductance without losing the quantization feature of Metal-Chern insulator-Metal setup.

5.2 Fourier transforming 2D SBHZ model in one direction gives 1D SSH chain

Since there is translation invariance in y-direction, we can do the Fourier transform in y-direction.

$$\Psi(x,y) = \frac{1}{\sqrt{N_y}} \sum_k e^{-iky} \Psi(x,k) \tag{5.6}$$

Putting this expression in Eq (5.1) and using the orthogonality condition $\sum_{y=1}^{N_y} e^{-i(k-k')y} = N_y \delta_{kk'}$, we get

$$\begin{aligned} H_W = & \sum_{x=1}^{N_x} \sum_k \mu_w \Psi^\dagger(x,k) \sigma_x \Psi(x,k) \\ & + \sum_{x=1}^{N_x} \sum_k \left[e^{-ik} \Psi^\dagger(x,k) \frac{1}{2} (\sigma_x - i\sigma_z) \Psi(x,k) + h.c. \right] \\ & + \sum_{x=1}^{N_x - 1} \sum_k \left[\Psi^\dagger(x,k) \frac{1}{2} (\sigma_x - i\sigma_y) \Psi(x+1,k) + h.c. \right] \end{aligned} \tag{5.7}$$

Hence, after re-arranging the terms, the Hamiltonian becomes,

$$\begin{aligned} H_W = & \sum_k \sum_{x=1}^{N_x} \Psi^\dagger(x,k) \left[(\mu_w + \cos k) \sigma_x + \sin k \ \sigma_z \right] \Psi(x,k) \\ & + \sum_k \sum_{x=1}^{N_x - 1} \left[\Psi^\dagger(x,k) \frac{1}{2} (\sigma_x - i\sigma_y) \Psi(x+1,k) + h.c. \right] \end{aligned} \tag{5.8}$$

$$\begin{aligned} H_W = & \sum_k \sum_{x=1}^{N_x} \Psi^\dagger(x,k) \begin{pmatrix} \sin k & \mu_w + \cos k \\ \mu_w + \cos k & -\sin k \end{pmatrix} \Psi(x,k) \\ & + \sum_k \sum_{x=1}^{N_x - 1} \left[\Psi^\dagger(x,k) \begin{pmatrix} 0 & 0 \\ 1 & 0 \end{pmatrix} \Psi(x+1,k) + h.c. \right] \end{aligned} \tag{5.9}$$

Diagrammatically this setup can be understood as shown in figure 5.2 . Hence, this Hamiltonian clearly represents sum of N_y uncoupled 1D chains of length N_x.

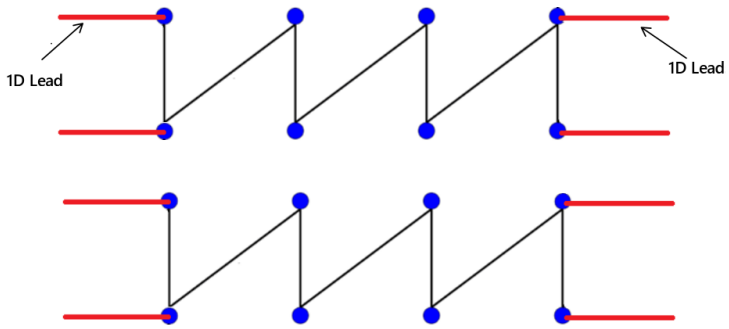

Figure 5.2: Fourier transformed metal-CI-metal setup

5.3 Defining the Hall Conductance in Cylindrical Geometry

The expression for current derived using continuity equation is given by following expression:

$$J_{\mathbf{x},\mathbf{x}'} = -2\mathrm{Im}\left\{H[\mathbf{x},\mathbf{x}']\langle\psi^\dagger(\mathbf{x})\psi(\mathbf{x}')\rangle\right\} \tag{5.10}$$

$$J_{\mathbf{x},\mathbf{x}'} = -2\mathrm{Im}\left\{H_W[\mathbf{x},a;\mathbf{x}',b]C_{\mathbf{x},a;\mathbf{x}',b}\right\} \tag{5.11}$$

Here, $C_{\mathbf{x},\mathbf{x}'}$ expression can be derived in NEGF formalism [11], and is given by:

$$C(\omega) = \int_{-\infty}^{\infty} C^L(\omega)f^L(\omega,\mu_L,T_L) + C^R(\omega)f^R(\omega,\mu_R,T_R) \tag{5.12}$$

Here, $C^{L/R} = 2\pi\mathcal{G}^+\Gamma_{L/R}\mathcal{G}^-$. Here $\mu_L = \mu + \Delta\mu_L$ and $\mu_R = \mu + \Delta\mu_R$. Here, $\Delta\mu_{L/R}$ is very small compared to μ or the relevant energy scale. **Note that we will consider $\Delta\mu_L = \Delta\mu$ and $\Delta\mu_R = 0$** in all further calculations. So,

$$f(\omega,\mu_{L/R}) = f(\omega,\mu) + f'(\omega,\mu)\Delta\mu_{L/R} + \mathcal{O}(\Delta\mu_{L/R}^2) \tag{5.13}$$

So, at 0K, we have

$$C(\omega) = \int_{-\infty}^{\mu} [C^L(\omega) + C^R(\omega)]d\omega + C^L(\omega)\Delta\mu_L + C^R(\omega)\Delta\mu_R \tag{5.14}$$

$$= C_{\text{equilibrium}} + C_{\text{excess}} \tag{5.15}$$

here,

$$C_{\text{equilibrium}} = \int_{-\infty}^{\mu} [C^L(\omega) + C^R(\omega)] d\omega \tag{5.16}$$

$$C_{\text{excess}} = C^L(\omega)\Delta\mu_L + C^R(\omega)\Delta\mu_R + \mathcal{O}((\Delta\mu_{L/R})^2) \tag{5.17}$$

Hence, current can also be written as:

$$J = J_{\text{equilibrium}} + J_{\text{excess}} \tag{5.18}$$

Differential conductance is defined by,

$$G = \lim_{\Delta\mu \to 0} \frac{\Delta J}{\Delta\mu} \tag{5.19}$$

where $\Delta J = J_{\text{total}} - J_{\text{equilibrium}}$. So, in the linear response regime, at 0K, Hall conductance can be defined as follows:

$$G_H(\mu) = \lim_{\Delta\mu \to 0} \frac{\sum_x \Delta J_{x,y \to x,y+1}}{\Delta\mu} \tag{5.20}$$

where y has some fixed value $\in \{1, 2, \cdots, N_y\}$. Due to the symmetry of the problem, we can also sum over y and divide by N_y which will help to simplify the analysis. So,

$$G_H(\mu) = \lim_{\Delta\mu \to 0} \frac{1}{N_y} \frac{\sum_{x,y} \Delta J_{x,y \to x,y+1}}{\Delta\mu} \tag{5.21}$$

$$= \frac{2}{N_y} \sum_{x,y} \sum_{a,b=1}^{2} \text{Im} \left\{ H_W[\mathbf{x}, a; \mathbf{x}', b] C^L_{\mathbf{x},a;\mathbf{x}',b} \right\} \tag{5.22}$$

$$= \frac{2}{N_y} \sum_{x,y} \sum_{a,b=1}^{2} \text{Im} \left\{ H_{x,y,a;\ x,y+1,b} C_{x,y,a;\ x,y+1,b} \right\} \tag{5.23}$$

From NEGF calculations we know that $C = C^L = 2\pi \mathcal{G}^+ \Gamma_L \mathcal{G}^-$ [13], hence

$$G_H = \frac{4\pi}{N_y} \text{Im} \sum_{x,y} \sum_{a,b=1}^{2} \left\{ H_{x,y,a;\ x,y+1,b} (\mathcal{G}^+ \Gamma_L \mathcal{G}^-)_{x,y,a;\ x,y+1,b} \right\} \tag{5.24}$$

5.4 Fourier transformation using unitary matrix

We will use the following order of basis to picture the matrix multiplications to obtain the expression for Hall conductance:

$$\{\Psi(1,1), \Psi(2,1), \cdots, \Psi(N_x,1), \Psi(1,2), \Psi(2,2)\cdots\Psi(N_x,2)\cdots\Psi(1,N_y), \cdots\Psi(N_x,N_y)\}$$

However, note that the derivation is done in a way such that the calculation is independent of basis.

Fourier transforming in y-direction is equivalent to applying the following unitary matrix:

$$\boxed{U_{x,y;x',y'} = \frac{1}{\sqrt{N_y}} e^{ik_{y'}y}\delta_{x,x'}} \tag{5.25}$$

Here, x, x' (y, y') and any other such variable only takes integer value upto N_x (N_y).
Here, $k_{y'} = \frac{2y'\pi}{N_y}$ To see that U is indeed unitary:

$$\begin{aligned}
(UU^\dagger)_{x,y;x',y'} &= \sum_{x_1,y_1} U_{x,y;x_1,y_1} U^\dagger_{x_1,y_1:x',y'} && (5.26)\\
&= \sum_{x_1,y_1} U_{x,y;x_1,y_1} U^*_{x',y':x_1,y_1} && (5.27)\\
&= \frac{1}{N_y}\sum_{x_1,y_1} e^{ik_{y_1}(y-y')}\delta_{x,x_1}\delta_{x',x_1} && (5.28)\\
&= \delta_{x,x'}\delta_{y,y'} && (5.29)
\end{aligned}$$

where, in the last line we used the orthogonality condition, $\sum_{y_1} e^{ik_{y_1}(y-y')} = N_y\delta_{y,y'}$.

5.5 Simplifying Hall conductance

$$G_H = \frac{4\pi}{N_y}\mathrm{Im}\sum_{x,y}\sum_{a,b=1}^{2}\left\{H^{ab}_{x,y;\ x,y+1}(\mathcal{G}^+\Gamma_L\mathcal{G}^-)^{ab}_{x,y;\ x,y+1}\right\} \tag{5.30}$$

Applying unitary transform, we get:

$$G_H = \frac{4\pi}{N_y}\mathrm{Im}\sum_{x,y}\sum_{a,b=1}^{2}\left\{H^{ab}_{x,y;\ x,y+1}(U(U^\dagger\mathcal{G}^+U)(U^\dagger\Gamma_R U)(U^\dagger\mathcal{G}^-U)U^\dagger)^{ab}_{x,y;\ x,y+1}\right\} \tag{5.31}$$

$$= \frac{4\pi}{N_y}\mathrm{Im}\sum_{x,y}\sum_{a,b=1}^{2}\left\{H^{ab}_{x,y;\ x,y+1}(U(\tilde{G}^+\tilde{\Gamma}\tilde{G}^-)U^\dagger)^{ab}_{x,y;\ x,y+1}\right\} \tag{5.32}$$

$$= \frac{4\pi}{N_y}\mathrm{Im}\sum_{x,y}\left\{\mathrm{tr}\left(H_{x,y;\ x,y+1}(U(\tilde{G}^+\tilde{\Gamma}\tilde{G}^-)U^\dagger)_{x,y;\ x,y+1}\right)\right\} \tag{5.33}$$

Here, tr() represents trace over intracell sites. Now, we will simplify one of the term inside trace.

$$(U(\tilde{G}^+\tilde{\Gamma}\tilde{G}^-)U^\dagger)_{x,y;\ x,y+1} = \sum_{x_1,y_1}\sum_{x_2,y_2}(U)_{x,y;x_1,y_1}(\tilde{G}^+\tilde{\Gamma}\tilde{G}^-)_{x_1,y_1;x_2,y_2}(U^\dagger)_{x_2,y_2;\ x,y+1} \tag{5.34}$$

$$= \frac{1}{N_y}\sum_{x_1,y_1}\sum_{x_2,y_2}(e^{ik_{y_1}y}\delta_{x,x_1})(\tilde{G}^+\tilde{\Gamma}\tilde{G}^-)_{x_1,y_1;x_2,y_2}(e^{-ik_{y_2}(y+1)}\delta_{x,x_2}) \tag{5.35}$$

$$= \frac{1}{N_y}\sum_{x_1,y_1}\sum_{x_2,y_2}(e^{ik_{y_1}y}e^{-ik_{y_2}(y+1)}\delta_{x,x_1}\delta_{x,x_2})(\tilde{G}^+\tilde{\Gamma}\tilde{G}^-)_{x_1,y_1;x_2,y_2}\delta_{y_1,y_2} \tag{5.36}$$

$$= \frac{1}{N_y}\sum_{y_1}(e^{-ik_{y_1}})(\tilde{G}^+\tilde{\Gamma}\tilde{G}^-)_{x,y_1;x,y_1} \tag{5.37}$$

In the third line, we put $\delta_{y,y'}$ because we know that $\tilde{G}^+\tilde{\Gamma}\tilde{G}^-$ is block diagonal (unitary transformation makes H and Σ block diagonal, see Appendix A).

Also note,

$$H_{x,y;x,y+1} = \frac{(\sigma_x + i\sigma_z)}{2} \tag{5.38}$$

so using (5.37) and (5.38), equation (5.33) simplifies to

$$G_H = \frac{2\pi}{N_y}\mathrm{Im}\left\{\sum_{x,y}\mathrm{tr}\left((\sigma_x + i\sigma_z)e^{-ik_y}(\tilde{G}^+\tilde{\Gamma}\tilde{G}^-)_{x,y;x,y}\right)\right\} \tag{5.39}$$

evaluating the imaginary part and simplifying the expression, we get

$$G_H = \frac{2\pi}{N_y} \sum_{x,y} \text{tr} \left\{ (\text{sin}k_y\sigma_x - \text{cos}k_y\sigma_z)(\tilde{G}^+(k_y)\tilde{\Gamma}\tilde{G}^-(k_y))_{x,y;x,y} \right\} \tag{5.40}$$

we define,

$$F(k_y) = \sigma_x \text{sin}k_y - \sigma_z \text{cos}k_y \tag{5.41}$$

$$C^{1D}_{xx}(k_y) = (\tilde{G}^+(k_y)\tilde{\Gamma}\tilde{G}^-(k_y))_{x,y;x,y} \tag{5.42}$$

Here, both $F(k_y)$ and $C^{1D}_{xx}(k_y)$ are 2×2 matrices and tr() is taken over intracell sites. So,

$$\boxed{G_H = \frac{2\pi}{N_y} \sum_{x,y} \text{tr} \left(F(k_y) C^{1D}_{xx}(k_y) \right)} \tag{5.43}$$

We can further simplify this expression as follows:

$$G_H = \frac{2\pi}{N_y} \sum_{x,y} \sum_{a,b} \left(F_{ab}(k_y)(\tilde{G}^+(k_y)\tilde{\Gamma}\tilde{G}^-(k_y))_{x,y,a;x,y,b} \right) \tag{5.44}$$

$$= \frac{2\pi}{N_y} \sum_{x,y} \sum_{x_1,y_1} \sum_{x_2,y_2} \sum_{a,b,c,d} \left(F_{ab}(k_y)(\tilde{G}^+(k_y))_{x,y,a;x_1,y_1,c}(\tilde{\Gamma})_{x_1,y_1,c;x_2,y_2,d}\tilde{G^-}(k_y)_{x_2,y_2,d;x,y,b} \right) \tag{5.45}$$

Using, $\tilde{\Gamma}_{x_1,y_1,c;x_2,y_2,d} = \frac{1}{\pi}\frac{\eta_c^2}{\eta_b}\delta_{x_1,x_2}\delta_{y_1,y_2}\delta_{cd}\delta_{1,x_1}$

$$G_H = \frac{2}{N_y}\frac{\eta_c^2}{\eta_b} \sum_{x,y} \sum_{x_1,y_1,x_2,y_2} \sum_{a,b,c,d} \left(F_{ab}(k_y)(\tilde{G}^+(k_y))_{x,y,a;x_1,y_1,c}\ \delta_{y,y_1}(\delta_{x_1,x_2}\delta_{y_1,y_2}\delta_{cd}\delta_{1,x_1})\tilde{G^-}(k_y)_{x_2,y_2,d;x,y,b}\ \delta_{y,y_2} \right) \tag{5.46}$$

$$= \frac{2}{N_y}\frac{\eta_c^2}{\eta_b} \sum_{x,y} \sum_{a,b,c} \left(F_{ab}(k_y)(\tilde{G}^+(k_y))_{x,y,a;1,y,c}\tilde{G^-}(k_y)_{1,y,c;x,y,b} \right) \tag{5.47}$$

$$\tag{5.48}$$

We define simpler notation:

$\mathcal{G}_{x,a;1,c} = \tilde{G}^{+}(k_y)_{x,y,a;1,y,c}$ and $(\mathcal{G}^{\dagger})_{1,c;x,b} = \tilde{G}^{-}(k_y)_{1,y,c;x,y,b}$

$$G_H = \frac{2}{N_y}\frac{\eta_c^2}{\eta_b}\sum_{x,y}\sum_{a,b,c}\left(F_{ab}(k_y)\mathcal{G}_{x,a;1,c}\ (\mathcal{G}^{\dagger})_{1,c;x,b}\right) \tag{5.49}$$

$$= \frac{2}{N_y}\frac{\eta_c^2}{\eta_b}\sum_{x,y}\mathrm{tr}(\mathcal{G}^{\dagger}_{x1}(k_y)F(k_y)\mathcal{G}_{x1}(k_y)) \tag{5.50}$$

We need to find $\mathcal{G}_{x1}$ which are 2×2 blocks of $\mathcal{G}(k_y)$. $\mathcal{G}(k_y)$ is the Green's function of 1D SBHZ in presence of reservoirs. Using numerics, we can verify that (5.50) indeed gives quantization as shown in figure 5.3.

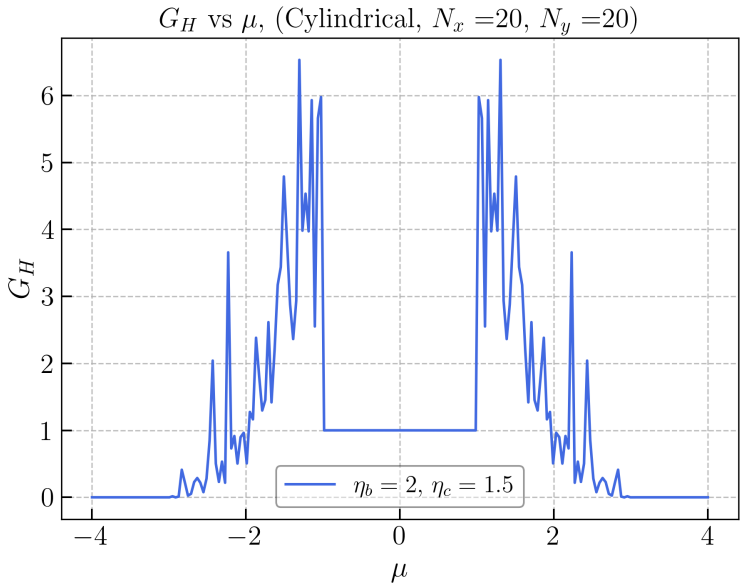

Figure 5.3: Hall Conductance as a function of μ using the Fourier transformed expression (Eq (5.50))

5.6 Further simplifying the setup

In order to obtain quantization of conductance in Chern insulator setup, we may not need reservoirs with 2 degrees of freedom. We can also consider the following connection of reservoir to Chern insulator which shows quantization and simplifies the transfer matrix analysis.

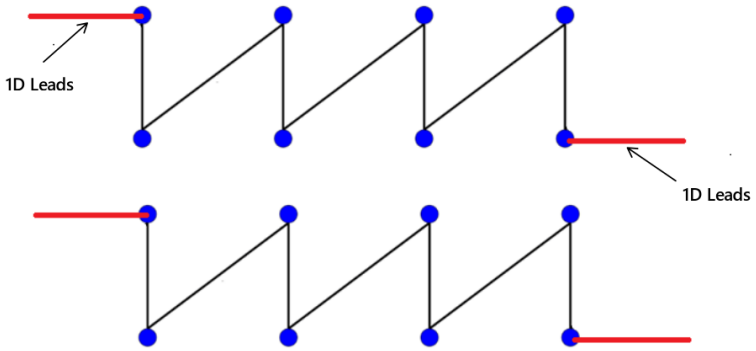

Figure 5.4: Simplified Metal-CI-Metal setup in Fourier basis

In this setup, $\tilde{\Gamma}_{x_1,y_1,c;x_2,y_2,d} = \frac{1}{\pi}\frac{\eta_c^2}{\eta_b}\delta_{x_1,x_2}\delta_{y_1,y_2}\delta_{1,x_1}\delta_{cd}\delta_{1c}$ (The only difference here from the old expression is the presence of δ_{1c})

This simplifies the Hall conductance expression to,

$$G_H = \frac{2}{N_y}\frac{\eta_c^2}{\eta_b}\sum_{x,y}\sum_{a,b}\left(F_{ab}(k_y)\mathcal{G}_{x,a;1,1}\ (\mathcal{G}^\dagger)_{1,1;x,b}\right) \tag{5.51}$$

$$= \frac{2}{N_y}\frac{\eta_c^2}{\eta_b}\sum_{x,y}\mathcal{G}^\dagger_{x1}(k_y)F(k_y)\mathcal{G}_{x1}(k_y) \tag{5.52}$$

where $\mathcal{G}_{x1} = \begin{pmatrix}\mathcal{G}_{x,1;1,1} & \mathcal{G}_{x,2;1,1}\end{pmatrix}^T = \begin{pmatrix}\mathcal{G}^1_{x,1} & \mathcal{G}^2_{x,1}\end{pmatrix}^T$

5.7 Transfer matrix for 1D SSH chain

From the Hamiltonian (in eq(5.9))and figure 5.4, we can conclude that the 2D Chern Insulator in cylindrical geometry is essentially a set of 1D SSH chains with staggered site potential. In this section, we will obtain Transfer Matrix for 1D SSH chain and will use it to obtain a simplified expression for Hall conductance.

Following is the matrix equation we need to solve:

$$(\omega - H_W - \Sigma_L - \Sigma_R)\mathcal{G}^+(\omega) = \mathbb{I} \tag{5.53}$$

$$\begin{pmatrix} \omega-a-\Sigma & -b & 0 & 0 & \cdots & 0 & 0 \\ -b & \omega+a & -1 & 0 & \cdots & 0 & 0 \\ 0 & -1 & \omega-a & -b & \cdots & 0 & 0 \\ \vdots & \vdots & -b & \omega+a & \ddots & \vdots & \vdots \\ \vdots & \vdots & \vdots & \ddots & \ddots & -1 & 0 \\ \vdots & \vdots & \vdots & \cdots & -1 & \omega-a & -b \\ 0 & 0 & 0 & \cdots & 0 & -b & \omega+a-\Sigma \end{pmatrix} \begin{pmatrix} \mathcal{G}^1_{11} & \cdots \\ \mathcal{G}^2_{11} & \cdots \\ \mathcal{G}^1_{21} & \cdots \\ \vdots & \cdots \\ \vdots & \cdots \\ \mathcal{G}^1_{N_x1} & \cdots \\ \mathcal{G}^2_{N_x1} & \cdots \end{pmatrix} = \begin{pmatrix} 1 & 0 & \cdots \\ 0 & 1 & \cdots \\ 0 & 0 & \cdots \\ \vdots & \vdots & \cdots \\ \vdots & \vdots & \cdots \\ 0 & 0 & \cdots \\ 0 & 0 & \cdots \end{pmatrix} \tag{5.54}$$

Here, $a = \sin k$, $b = \mu_w + \cos k$ (see eq 5.9) and $\Sigma = \frac{-i\eta_c^2}{\eta_b}$. First column of RHS and LHS give us the following set of equations[1]:

$$(\omega - a - \Sigma)\mathcal{G}^1_{11} - b\mathcal{G}^2_{11} = 1 \tag{5.55}$$

$$-b\mathcal{G}^1_{x-1,1} + (\omega + a)\mathcal{G}^2_{x-1,1} - \mathcal{G}^1_{x,1} = 0 \quad (2 \le x \le N) \tag{5.56}$$

$$-\mathcal{G}^1_{x-1,1} + (\omega - a)\mathcal{G}^1_{x,1} - b\mathcal{G}^2_{x,1} = 0 \quad (2 \le x \le N) \tag{5.57}$$

$$-b\mathcal{G}^1_{N1} + (\omega + a - \Sigma)\mathcal{G}^2_{N1} = 0 \tag{5.58}$$

[1]Note $N = N_x$

These equations can be rewritten in matrix form as follows:

$$\begin{pmatrix} 1 \\ \mathcal{G}^1_{11} \end{pmatrix} = \begin{pmatrix} \omega - a - \Sigma & -b \\ 1 & 0 \end{pmatrix} \begin{pmatrix} \mathcal{G}^1_{11} \\ \mathcal{G}^2_{11} \end{pmatrix} \tag{5.59}$$

$$\begin{pmatrix} \mathcal{G}^1_{x-1,1} \\ \mathcal{G}^2_{x-1,1} \end{pmatrix} = \begin{pmatrix} \frac{(\omega^2-a^2)-1}{b} & -(\omega+a) \\ \omega - a & -b \end{pmatrix} \begin{pmatrix} \mathcal{G}^1_{x,1} \\ \mathcal{G}^2_{x,1} \end{pmatrix} \qquad (2 \leq x \leq N) \tag{5.60}$$

$$\begin{pmatrix} \mathcal{G}^1_{N1} \\ \mathcal{G}^2_{N1} \end{pmatrix} = \begin{pmatrix} \frac{\omega+a-\Sigma}{b} & -1 \\ 1 & 0 \end{pmatrix} \begin{pmatrix} \mathcal{G}^2_{N1} \\ 0 \end{pmatrix} \tag{5.61}$$

We will use the following notation for the matrices:

$$\Omega_L = \begin{pmatrix} \omega - a - \Sigma & -b \\ 1 & 0 \end{pmatrix} \quad \Omega = \begin{pmatrix} \frac{(\omega^2-a^2)-1}{b} & -(\omega+a) \\ \omega - a & -b \end{pmatrix} \quad \Omega_R = \begin{pmatrix} \frac{\omega+a-\Sigma}{b} & -1 \\ 1 & 0 \end{pmatrix} \tag{5.62}$$

$$\mathcal{G}_{x1} = \begin{pmatrix} \mathcal{G}^1_{x,1} \\ \mathcal{G}^2_{x,1} \end{pmatrix} \tag{5.63}$$

$$\boxed{\begin{pmatrix} 1 \\ \mathcal{G}^1_{11} \end{pmatrix} = \Omega_L \mathcal{G}_{x1} \quad ; \quad \mathcal{G}_{x-1,1} = \Omega\ \mathcal{G}_{x,1} \quad (2 \leq x \leq N) \quad ; \quad \mathcal{G}_{N1} = \Omega_R \begin{pmatrix} \mathcal{G}^2_{N1} \\ 0 \end{pmatrix}} \tag{5.64}$$

Note that the transfer matrix elements have $\mathbf{b = (\mu_w + \cos k)}$ in the denominator. Hence, for $\mu_w \in (-1, 1)$ transfer matrix will not be well-defined as denominator can become zero for certain value of k. Since the non-trival topological regime is $-2 < \mu_w < 2$, transfer matrix can still be used to capture quantization when $1 < |\mu_w| < 2$. Hence, in further sections, we will take $\mu_w = 1.1$ to prevent denominator from blowing up.

5.8 Hall conductance using transfer matrix

Using equation(5.64), we can write the following equations:

$$\mathcal{G}_{x1} = \Omega^{N-x} \mathcal{G}_{N1} \tag{5.65}$$

$$\mathcal{G}^{\dagger}_{x1} = \mathcal{G}^{\dagger}_{N1}(\Omega^{\dagger})^{N-x} \tag{5.66}$$

We can use these equations to simplify the expression for Hall Conductance as follows:

$$G_H = \frac{2}{N_y}\frac{\eta_c^2}{\eta_b}\sum_{x,y}\mathcal{G}^{\dagger}_{x1}(k_y)F(k_y)\mathcal{G}_{x1}(k_y) \tag{5.67}$$

$$= \frac{2}{N_y}\frac{\eta_c^2}{\eta_b}\sum_{x,y}\mathcal{G}^{\dagger}_{N1}\left[(\Omega^{\dagger})^{N-x}F(k_y)\Omega^{N-x}\right]\mathcal{G}_{N1} \tag{5.68}$$

$$\tag{5.69}$$

Obtaining $\mathbf{G_{N1}}$

Using eq(5.64) and eq(5.65), we can write

$$\begin{pmatrix}1\\ \mathcal{G}^1_{11}\end{pmatrix} = \Omega_L\Omega^{N-1}\Omega_R\begin{pmatrix}\mathcal{G}^2_{N1}\\ 0\end{pmatrix} \tag{5.70}$$

Let $\boxed{\tilde{\Omega} = \Omega_L\Omega^{N-1}\Omega_R}$

$$\begin{pmatrix}1\\ \mathcal{G}^1_{11}\end{pmatrix} = \begin{pmatrix}\tilde{\Omega}_{11} & \tilde{\Omega}_{12}\\ \tilde{\Omega}_{21} & \tilde{\Omega}_{22}\end{pmatrix}\begin{pmatrix}\mathcal{G}^2_{N1}\\ 0\end{pmatrix} \tag{5.71}$$

So,

$$\boxed{\mathcal{G}^2_{N1} = \tilde{\Omega}^{-1}_{11}} \tag{5.72}$$

From eq(5.58), we also have,

$$-b\mathcal{G}^1_{N1} + (\omega + a - \Sigma)\mathcal{G}^2_{N1} = 0 \tag{5.73}$$

Hence,

$$\mathcal{G}_{1N} = \begin{pmatrix}\mathcal{G}^1_{N1}\\ \mathcal{G}^2_{N1}\end{pmatrix} = \mathcal{G}^2_{N1}\begin{pmatrix}\frac{(\omega+a-\Sigma)}{b}\\ 1\end{pmatrix} := |\Phi_{k_y}\rangle \tag{5.74}$$

We can now write the Hall conductance (eq(5.68)) solely in terms of 2×2 transfer matrix and its elements:

$$G_H = \frac{2}{N_y}\frac{\eta_c^2}{\eta_b}\sum_{x,y}\langle\Phi_{k_y}|(\Omega^{\dagger})^{N-x}F(k_y)\Omega^{N-x}|\Phi_{k_y}\rangle \tag{5.75}$$

Note here, $a = \sin k$ and $b = \mu_w + \cos k$.

5.9 Analysis at $\mu = 0$

In order to understand the quantization of Hall conductance as we approach thermodynamic limit, we fix the fermi level to $\mu = 0$ which simplifies our transfer matrix expressions as follows:

$$\Omega_L = \begin{pmatrix} -a-\Sigma & -b \\ 1 & 0 \end{pmatrix} \quad \Omega = \begin{pmatrix} c & -a \\ -a & -b \end{pmatrix} \quad \Omega_R = \begin{pmatrix} \frac{a-\Sigma}{b} & -1 \\ 1 & 0 \end{pmatrix} \tag{5.76}$$

Here, $c = \frac{-(a^2+1)}{b}$, $a = \sin k$ and $b = \mu_w + \cos k$.

We want to show that as we increase N_y, Hall conductance, G_H approaches to 1.

We can spectral decompose the transfer matrix using projection operators corresponding to each eigenvalue.

$$\Omega = \lambda_1 P_1 + \lambda_2 P_2 \quad \text{where} \quad P_i P_j = \delta_{ij} P_i \tag{5.77}$$

Note that, $\lambda_1 \lambda_2 = 1$ since $\mathrm{Det}(\Omega) = 1$. From here on, we will assume $|\lambda_1| < 1$ and $|\lambda_2| > 1$.

At μ= 0, eq (5.75) can be rewritten in a compact form in the following new notation ($k = k_y, N = N_x$):

$$G_H = \frac{2}{N_y} \frac{\eta_c^2}{\eta_b} \sum_k \langle \tilde{\Phi}_k | M(k) | \tilde{\Phi}_k \rangle \tag{5.78}$$

where,

$$M(k) = |\mathcal{G}_{N1}^2|^2 \times \sum_{x=1}^{N} (\Omega^\dagger)^{N-x} F(k) \Omega^{N-x} \tag{5.79}$$

and

$$|\tilde{\Phi}_k\rangle := \begin{pmatrix} \frac{(\omega+a-\Sigma)}{b} \\ 1 \end{pmatrix} \tag{5.80}$$

Using eq(5.77), we can simplify the sum in eq(5.79) as,

$$\sum_{x=1}^{N_x} (\Omega^\dagger)^{N-x} F(k_y) \Omega^{N-x} = \sum_{x=1}^{N_x} (\lambda_1 P_1 + \lambda_2 P_2)^{N-x} \times F \times (\lambda_1 P_1 + \lambda_2 P_2)^{N-x} \tag{5.81}$$

$$= \sum_{x=1}^{N_x} \left[(\lambda_1)^{2(N-x)} P_1 F P_1 + (\lambda_2)^{2(N-x)} P_2 F P_2 + P_1 F P_2 + P_2 F P_1 \right] \tag{5.82}$$

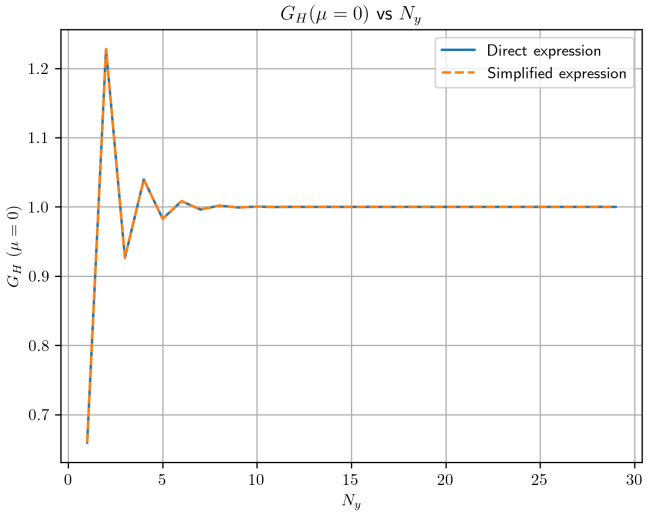

Figure 5.5: Hall conductance(G_H) vs N_y plot which indicates that G_H quantizes to 1 in the thermodynamic limit. This plot also numerically verifies that the simplified expression obtained in equation (5.78) till (5.87) are correct by comparing it with the plot obtained using formal expression given in eq. (5.52).

And we know that $\mathcal{G}^2_{N1} = \tilde{\Omega}^{-1}_{11}$ where $\tilde{\Omega} = \Omega_L \Omega^{N-1} \Omega_R$

$$\tilde{\Omega}_{11} = (\Omega_L \Omega^{N-1} \Omega_R)_{11} \tag{5.83}$$

$$= [\lambda_1^{N-1} (\Omega_L P_1 \Omega_R)_{11} + \lambda_2^{N-1} (\Omega_L P_2 \Omega_R)_{11}] \tag{5.84}$$

$$= [\lambda_1^{N-1} \alpha + \lambda_2^{N-1} \beta] \tag{5.85}$$

where we defined $\alpha = (\Omega_L P_1 \Omega_R)_{11}$ and $\beta = (\Omega_L P_2 \Omega_R)_{11}$. So,

$$|\mathcal{G}^2_{N1}|^2 = \frac{1}{|\tilde{\Omega}_{11}|^2} = \frac{1}{[|\alpha|^2 \lambda_1^{2(N-1)} + |\beta|^2 \lambda_2^{2(N-1)} + \alpha^* \beta + \alpha \beta^*]} \tag{5.86}$$

$$M(k_y) = \frac{1}{|\tilde{\Omega}_{11}|^2} \times \sum_{x=1}^{N_x} \left[(\lambda_1)^{2(N-x)} P_1 F P_1 + (\lambda_2)^{2(N-x)} P_2 F P_2 + P_1 F P_2 + P_2 F P_1 \right] \tag{5.87}$$

$$= \frac{1}{|\tilde{\Omega}_{11}|^2} \times \left\{ \frac{\lambda_1^{2(N_x-1)} (1 - \lambda_1^{-2N_x})}{1 - \lambda_1^{-2}} P_1 F P_1 + \frac{\lambda_2^{2(N_x-1)} (1 - \lambda_2^{-2N_x})}{1 - \lambda_2^{-2}} P_2 F P_2 + N_x (P_1 F P_2 + P_2 F P_1) \right\} \tag{5.88}$$

5.9.1 $N_y \to \infty$ limit

In the limit $N_y \to \infty$, we can convert the summation over k to an integral,

$$G_H = \frac{2}{N_y}\frac{\eta_c^2}{\eta_b}\sum_k \langle\tilde{\Phi}_k|M(k)|\tilde{\Phi}_k\rangle \tag{5.89}$$

Using this expression and the fact that $\Delta k = \Delta k_y = k_{y+1} - k_y = \frac{2\pi}{N_y}$, we obtain (in the limit $N_y \to \infty$)

$$G_H = \frac{1}{\pi}\frac{\eta_c^2}{\eta_b}\int_0^{2\pi} \langle\tilde{\Phi}_k|M(k)|\tilde{\Phi}_k\rangle \;\; dk \tag{5.90}$$

5.9.2 $N_x \to \infty$ limit

In the equation (5.90), only $M(k)$ have N_x dependence. We will analyze the coefficient of each term in the expression of $M(k)$ separately (using eq. (5.87)) :

Term-1 coefficient:

$$\frac{(\lambda_1)^{2(N-x)}}{[|\alpha|^2\lambda_1^{2(N-1)} + |\beta|^2\lambda_2^{2(N-1)} + \alpha^*\beta + \alpha\beta^*]} \tag{5.91}$$

Multiplying numerator and denominator by $(\lambda_1)^{-2N}$, we get

$$\frac{(\lambda_1)^{-2x}}{[|\alpha|^2\lambda_1^{-2} + |\beta|^2\lambda_1^{-4N+2} + \lambda_1^{-2N}(\alpha^*\beta + \alpha\beta^*)]} = 0 \quad \text{in the limit} \;\; N \to \infty \tag{5.92}$$

Term-2 coefficient:

$$\frac{(\lambda_2)^{2(N-x)}}{[|\alpha|^2\lambda_1^{2(N-1)} + |\beta|^2\lambda_2^{2(N-1)} + \alpha^*\beta + \alpha\beta^*]} \tag{5.93}$$

Multiplying numerator and denominator by $(\lambda_2)^{-2N}$, we get

$$\frac{(\lambda_2)^{-2x}}{[|\alpha|^2\lambda_1^{4N-2}+|\beta|^2\lambda_2^{-2}+\lambda_1^{2N}(\alpha^*\beta+\alpha\beta^*)]}=\frac{1}{|\beta|^2}\lambda_2^{-2(x-1)} \quad \text{in the limit} \quad N\to\infty \tag{5.94}$$

Term-3 and 4 coefficient:

$$\frac{N}{[|\alpha|^2\lambda_1^{2(N-1)}+|\beta|^2\lambda_2^{2(N-1)}+\alpha^*\beta+\alpha\beta^*]} \tag{5.95}$$

Multiplying numerator and denominator by $(\lambda_2)^{-2N}$, we get

$$\frac{N(\lambda_2)^{-2N}}{[|\alpha|^2\lambda_1^{4N-2}+|\beta|^2\lambda_2^{-2}+\lambda_1^{2N}(\alpha^*\beta+\alpha\beta^*)]}=0 \quad \text{in the limit} \quad N\to\infty \tag{5.96}$$

So,

$$M(k_y)=\frac{1}{|\beta|^2}\left(\lim_{N\to\infty}\sum_{x=1}^{N}\lambda_2^{-2(x-1)}\right)P_2FP_2 \tag{5.97}$$

$$=\frac{1}{|\beta|^2}\left(\lim_{N\to\infty}\sum_{x=1}^{N}\lambda_1^{2(x-1)}\right)P_2FP_2 \tag{5.98}$$

$$=\frac{1}{|\beta|^2}\frac{1}{1-\lambda_1^2}\;\;P_2FP_2 \tag{5.99}$$

Hence, Hall conductance expression (5.90) simplifies to:

$$G_H=\frac{1}{\pi}\frac{\eta_c^2}{\eta_b}\int_0^{2\pi}\frac{dk}{|\beta|^2}\frac{1}{1-\lambda_1^2}\;\;\langle\tilde{\Phi}_k|P_2FP_2|\tilde{\Phi}_k\rangle \tag{5.100}$$

Using $P_2=|\lambda_2\rangle\langle\lambda_2|$, we can rewrite the expression as,

$$G_H=\frac{\gamma}{\pi}\int_0^{2\pi}\frac{dk}{|\beta|^2}\frac{1}{1-\lambda_1^2}\;\;\langle\tilde{\Phi}_k|\lambda_2\rangle\langle\lambda_2|F(k)|\lambda_2\rangle\langle\lambda_2|\tilde{\Phi}_k\rangle \tag{5.101}$$

$$=\frac{\gamma}{\pi}\int_0^{2\pi}\frac{dk}{|\beta|^2}\frac{1}{1-\lambda_1^2}\;\;|\langle\tilde{\Phi}_k|\lambda_2\rangle|^2\langle\lambda_2|F(k)|\lambda_2\rangle \tag{5.102}$$

$$\tag{5.103}$$

A straightforward calculation shows that,

$$\beta = -b|\langle\tilde{\Phi}_k|\lambda_2\rangle|^2 \tag{5.104}$$

which also implies that β is real. This relation further simplifies the Hall conductance expression:

$$G_H = \frac{\gamma}{\pi}\int_0^{2\pi} dk\ \frac{1}{b(k)\beta(k)}\ \frac{1}{\lambda_1^2(k)-1}\ \langle\lambda_2|F(k)|\lambda_2\rangle \tag{5.105}$$

To recall, λ_1 is the eigenvalue of transfer matrix with magnitude less than 1. P_2 is the projection operator corresponding to eigenvalue λ_2 ($|\lambda_2| > 1$). β is (1, 1) element of the matrix $\Omega_L P_2 \Omega_R$, $b(k) = \mu_w + \cos(k)$, $F(k) = \sigma_x \sin(k) - \sigma_z \cos(k)$.

5.10 Hall conductance is quantized independent of coupling

Equation (5.100) gives us a simple analytic expression for Hall conductance of Metal-Chern insulator-Metal setup in the thermodynamic-limit. Although doing further simplification of this expression is still cumbersome, evaluating it numerically is very easy. Let $\gamma = \frac{\eta_c^2}{\eta_b}$, which is the parameter having information about how the reservoir is coupled to Chern insulator.

Numerical evaluation confirms the integral equals 1 over a wide range of coupling, though the integrand crucially depends on coupling. Figure 5.6 shows numerical plots of the integrand vs. k for different coupling values. When $\mu_w = 1.1$ (topological regime), the integrand becomes sharply peaked at $k = \pi$ at extremely small γ (less than 0.01). Also, when γ is very large (greater than 100), integrand peaks at $k = 0$ and 2π as suggested in figure above. This makes numerical evaluation of the integral difficult at very small and large values of γ. However, typical range of γ is between 0.5 to 5. We numerically verified the value of G_H using eq. (5.100) which is equal to 1 (atleast till 12 decimal places) for $\gamma \in [0.01, 100]$. This indicates that Hall conductance is indeed quantized in an open system setup and is independent of the junction details. The connection of this integral expression to some topological invariant is expected (due to robustness) however, not yet found by us.

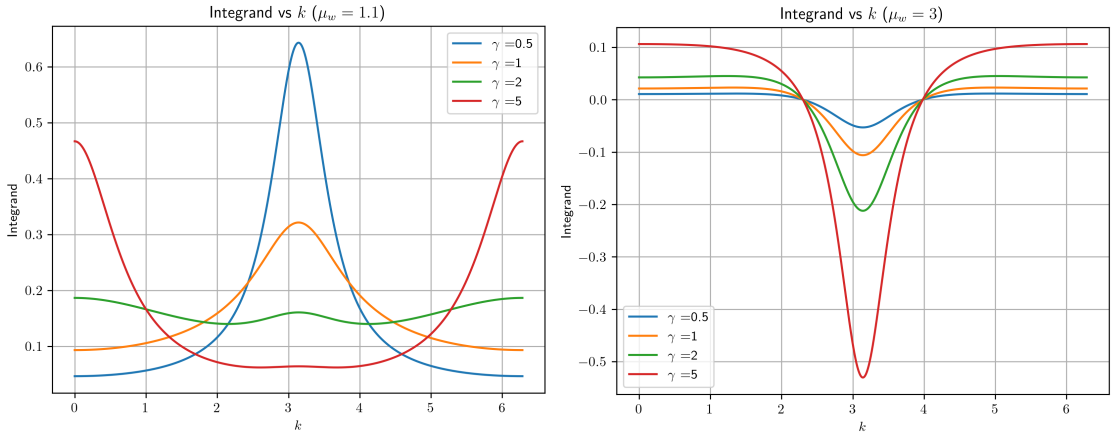

Figure 5.6: Integrand of Hall conductance expression as a function of k. Left: $\mu_w = 1.1$ (Chern number =1), Right: $\mu_w = 3$ (Chern number =0). The area under these curves for left (right) figure is always equal to 1 (0) independent of the shape of the curve (which delpends on coupling γ).

5.11 Analytical proof in the weak coupling limit

In this section, we analytically show that the obtained Hall conductance expression for an open setup is quantized in the topological regime (in the $\gamma \to 0$ limit).

The simplified expression for Hall conductance is given by:

$$G_H = \frac{\gamma}{\pi} \int_0^{2\pi} dk \, \frac{1}{b\beta} \times \frac{1}{\lambda_1^2 - 1} \times \langle \lambda_2 | F(k_y) | \lambda_2 \rangle \tag{5.106}$$

So, essentially there are 3 terms in this expression. Recall, $a(k) = \sin k$, $b(k) = \mu_w + \cos k$ and $\beta = (\Omega_L P_2 \Omega_R)_{11}$. $|\lambda_2\rangle$ satisfies the following equation:

$$\Omega |\lambda_2\rangle = \lambda_2 |\lambda_2\rangle \tag{5.107}$$

$$\begin{pmatrix} \frac{-(a^2+1)}{b} & -a \\ -a & -b \end{pmatrix} \begin{pmatrix} v_1 \\ v_2 \end{pmatrix} = \lambda_2 \begin{pmatrix} v_1 \\ v_2 \end{pmatrix} \tag{5.108}$$

Solving the eigenvalue equation for transfer matrix Ω, we get:

$$\lambda_\pm = -g(k) \pm \sqrt{g(k)^2 - 1} \tag{5.109}$$

where,

$$g(k) = \frac{a^2 + b^2 + 1}{2b} \tag{5.110}$$

λ_2 is defined as the eigenvalue having magnitude greater than 1.
We can simplify the first and last terms as follows:

Term 1:
It is easy to show that:

$$\frac{1}{\beta b} = -\frac{-1}{\gamma^2 v_1^2 + (av_1 + bv_2)^2} \tag{5.111}$$

Term 3:

$$\langle \lambda_2 | F(k_y) | \lambda_2 \rangle = \begin{pmatrix} v_1 & v_2 \end{pmatrix} \begin{pmatrix} -\cos(k_y) & \sin(k_y) \\ \sin(k_y) & \cos(k_y) \end{pmatrix} \begin{pmatrix} v_1 \\ v_2 \end{pmatrix} \tag{5.112}$$

$$= \begin{pmatrix} v_1 & v_2 \end{pmatrix} \begin{pmatrix} -(b - \mu_w) & a \\ a & (b - \mu_w) \end{pmatrix} \begin{pmatrix} v_1 \\ v_2 \end{pmatrix} \tag{5.113}$$

$$= (\mu_w - b)(v_1^2 - v_2^2) + 2av_1v_2 \tag{5.114}$$

Putting all three terms together, we get:

$$G_H = \frac{1}{\pi} \int_0^{2\pi} dk \; \frac{\gamma}{\gamma^2 v_1^2 + (av_1 + bv_2)^2} \; \frac{1}{\lambda_1^2 - 1} \; [(\mu_w - b)(v_1^2 - v_2^2) + 2av_1v_2] \tag{5.115}$$

Let, $v_2 = f(k_y)v_1$, then the expression simplifies to:

$$G_H = \frac{\gamma}{\pi} \int_0^{2\pi} dk \; \frac{1}{\gamma^2 + (a + bf)^2} \; \frac{1}{\lambda_1^2 - 1} \; [(\mu_w - b)(1 - f^2) + 2af] \tag{5.116}$$

Here, $f(k) = \frac{v_2}{v_1}$ can be obtained from second row of eq.(5.108) which gives:

$$f(k) = \frac{-a(k)}{\lambda_2 + b(k)} \tag{5.117}$$

We know from the numerical plot in fig. 5.6 that it peaks around $k = \pi$ (in topological regime) for small γ. Hence, we can expand the integrand around $k = \pi$ to obtain the leading contribution. We will change variable $k \to k - \pi$ to use the expansion around $k = 0$ instead

of $k = \pi$. So,

$$G_H = \frac{\gamma}{\pi}\int_{-\pi}^{\pi} dk \frac{1}{\gamma^2 + (a+bf)^2} \times \frac{1}{\lambda_1^2 - 1} \times [(\mu_w - b)(1-f^2) + 2af] \tag{5.118}$$

Now, $a = -\sin k$ and $b = \mu_w - \cos k$. In the above expression, let

$$a + bf = A(k) = A(0) + A'(0)k + \mathcal{O}(k^2) \tag{5.119}$$

$$\frac{1}{\lambda_1^2 - 1} = B(k) = B(0) + \mathcal{O}(k) \tag{5.120}$$

$$(\mu_w - b)(1-f^2) + 2af = C(k) = C(0) + \mathcal{O}(k) \tag{5.121}$$

For $0 < \mu_w < 2$, it can be shown that $A(0) = 0$. So, using series expansion of A, B and C functions, we get

$$G_H = \frac{\gamma^2}{\pi}\int_{-\pi}^{\pi} dk \ \frac{1}{\gamma^2 + [A'(0)k + \mathcal{O}(k^2)]^2} \ \times \ [B(0) + \mathcal{O}(k)] \ \times \ [C(0) + \mathcal{O}(k)] \tag{5.122}$$

Substituting $k = \gamma\tilde{k}$, we get

$$G_H = \frac{\gamma^2}{\pi}\int_{-\pi/\gamma}^{\pi/\gamma} d\tilde{k} \ \frac{1}{\gamma^2 + \left[A'(0)\gamma\tilde{k} + \mathcal{O}(\gamma^2\tilde{k}^2)\right]^2} \ \times \ [B(0) + \mathcal{O}(\gamma\tilde{k})] \ \times \ [C(0) + \mathcal{O}(\gamma\tilde{k})] \tag{5.123}$$

$$= \frac{1}{\pi}\int_{-\pi/\gamma}^{\pi/\gamma} d\tilde{k} \ \frac{1}{1 + \left[A'(0)\tilde{k} + \mathcal{O}(\gamma\tilde{k}^2)\right]^2} \ \times \ [B(0) + \mathcal{O}(\gamma\tilde{k})] \ \times \ [C(0) + \mathcal{O}(\gamma\tilde{k})] \tag{5.124}$$

$$\tag{5.125}$$

Taking the limit $\gamma \to 0$, we get

$$G_H = \frac{1}{\pi}\int_{-\infty}^{\infty} d\tilde{k} \ \frac{1}{1 + A'(0)^2\tilde{k}^2} \ \times \ B(0) \ \times \ C(0) \tag{5.126}$$

By a straightforward calculation, it can be shown that $B(0) = -A'(0) = \alpha$ and $C(0) = 1$. The resulting integral can be easily evaluated as follows:

$$G_H = \frac{1}{\pi}\int_{-\infty}^{\infty} dk\ \frac{\alpha}{1+\alpha^2 k^2} \tag{5.127}$$

$$= \frac{1}{\pi\alpha}\int_{-\infty}^{\infty} dk\ \frac{1}{(\frac{1}{\alpha})^2 + k^2} \tag{5.128}$$

$$= \frac{1}{\pi\alpha} \times \alpha \times \left[\tan^{-1}(k\alpha)\right]_{-\infty}^{\infty} \tag{5.129}$$

$$= 1 \tag{5.130}$$

Hence, we showed that in the regime $0 < \mu_w < 2$, Hall conductance is equal to 1.

Chapter 6

Some other numerical results

In this chapter, we will present two numerical results which arised out of the following two questions:

1) Hofstadter model represents a typical Quantum Hall System. If we connect metallic leads to this system, can we numerically observe quantization of two-terminal conductance(G_2) like we observe in the Chern insulator setup? To what values does the G_2 quantizes in this setup?

2) At $\mu = 0$, Chern insulator setup shows an interesting current pattern, as shown in ref. [13]. The current pattern observed there is expected due to square Fermi surface at $\mu = 0$ and single channel available due to edge state of Chern insulator. Can we obtain a similar current pattern in a normal tight-binding setup with no topological features?

6.1 Quantization in Hofstadter model

The Hofstadter model describe electrons in a two-dimensional lattice under the influence of a uniform magnetic field. The Hamiltonian of the Hofstadter model on a square lattice (with lattice spacing, $a = 1$) is given by:

$$H = -t \sum_{m,n} \left(c^{\dagger}_{x+1,y} c_{x,y} + e^{i2\pi\alpha x} c^{\dagger}_{x,y+1} c_{x,y} + \text{h.c.} \right), \tag{6.1}$$

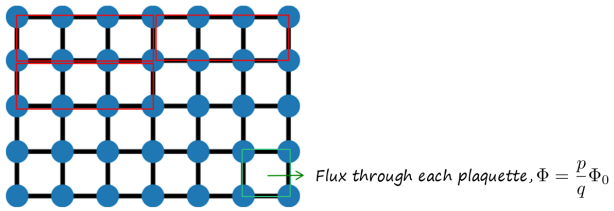

Figure 6.1: $6a \times 4a$ Hofstadter lattice, where magnetic flux through plaquettes leads to a sublattice structure. Suppose, for the lattice shown, $\frac{p}{q} = \frac{1}{3}$. Then the model essentially is a $2a \times 4a$ lattice with 3 degrees of freedom at each site as shown here.

where:

- $c^{\dagger}_{x,y}$ ($c_{x,y}$) is the creation (annihilation) operator for an electron at lattice site (x, y). t is the hopping amplitude between nearest-neighbor sites. The phase factor $e^{i2\pi\alpha x}$ arises from the Peierls substitution, which accounts for the effect of the magnetic field.
- $\alpha = \frac{\Phi}{\Phi_0}$ is the dimensionless magnetic flux per plaquette, with Φ being the magnetic flux through each plaquette and $\Phi_0 = \frac{h}{e}$, the magnetic flux quantum. We would always take magnetic flux to be rational and of the form, $\Phi = \frac{p}{q}\Phi_0$. So, $\alpha = \frac{p}{q}$.

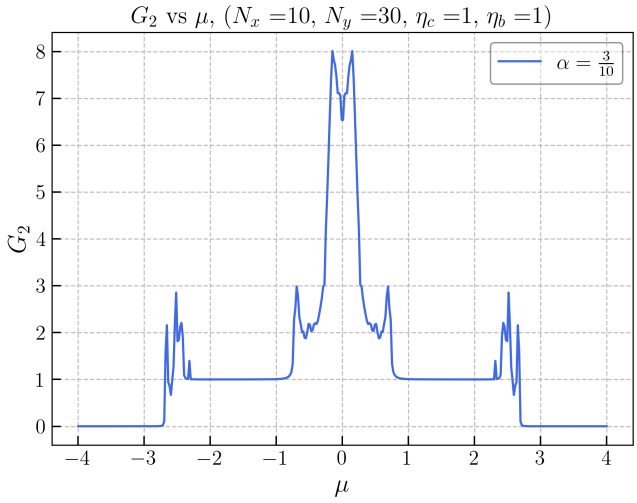

Figure 6.2: Numerical verification of quantization of G_2 in Hofstadter Model for $\alpha = \frac{3}{10}$

Using the NEGF formalism (summarized in section 3.3), one can numerically obtain G_2 vs μ plot for Hofstadter model connected to metallic leads. As expected, we observe quantization of two-terminal conductance in Hostadter model as shown in fig. 6.2.

6.1.1 Conductance plot for different α (flux)

Hofstadter model's spectrum crucially depends on the α parameter. It has a very rich spectrum (called Hofstader's butterfly) where bands can take different Chern number depending on the value of α. We get different number of pleataux if we change the flux through the lattice. In particular, for $\alpha = \frac{1}{5}$ and $\alpha = \frac{1}{6}$, we get two sets of plateau quantizing to values 1 and 2 (see fig. 6.3).

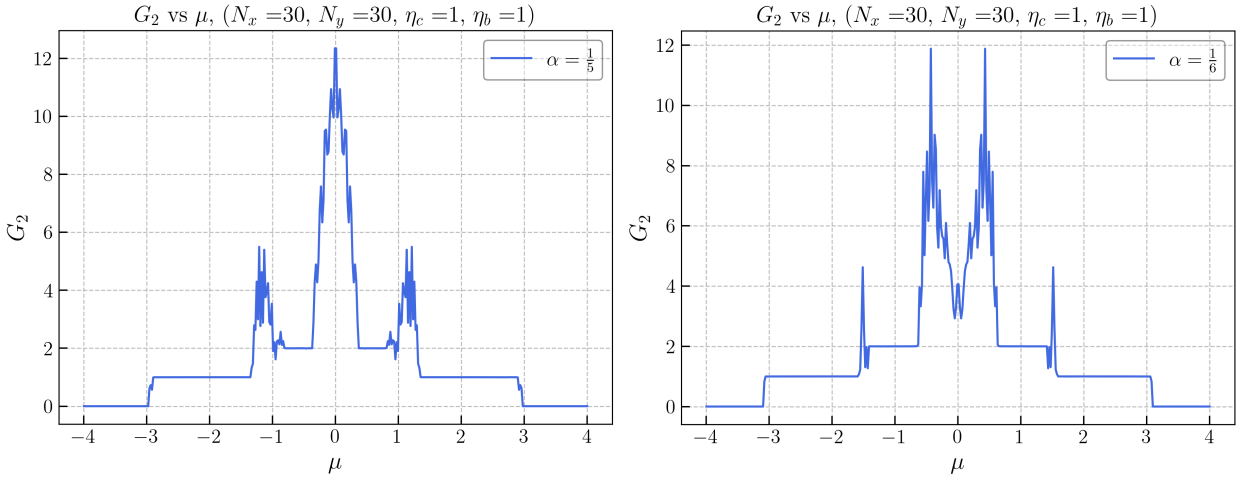

Figure 6.3: G vs μ plots for $\alpha = \frac{1}{5}$ (left) and $\alpha = \frac{1}{6}$ (right). Parameter values: $\eta_b = \eta_c = 1$, $N_x = N_y = 30$

6.2 Current pattern in 1D chain connected to 2D reservoirs

The Chern insulator setup shows interesting current pattern at $\mu = 0$. See the figure below taken from ref. [13]. The localized nature of current in reservoirs is due to the square fermi surface at $\mu = 0$ and because the current gets injected at the corner of Chern insulator. So, can such current pattern be observed in a setup with no topological features? To answer this, we consider setup shown in the figure below:

For such setup (which is implemented using KWANT python package), we observe the

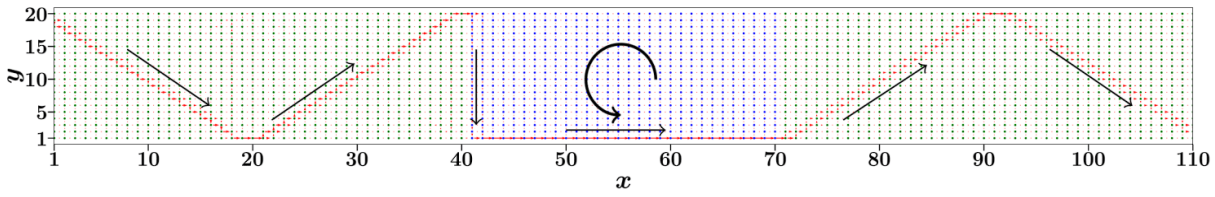

Figure 6.4: Current pattern in Chern insulator setup at $\mu = 0$. Region with blue sites represents Chern insulator and region with green sites represents reservoirs.

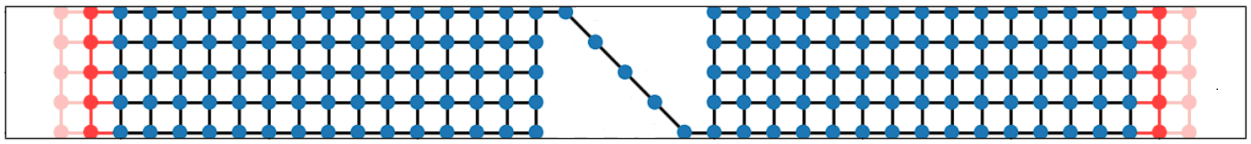

Figure 6.5: Schematic setup for a 1D tight binding wire diagonally connected to 2D reservoirs

following current pattern: Note that fig. 6.6 is a coarse grained version of the current pattern

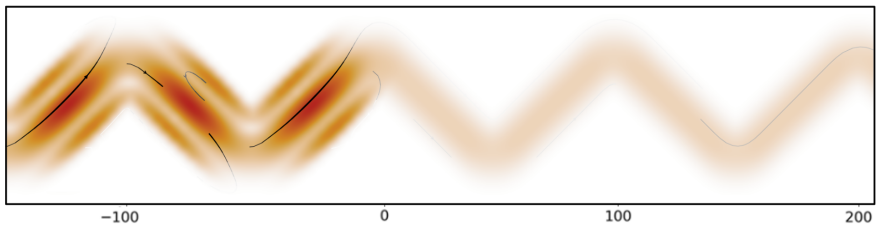

Figure 6.6: Current pattern in a tight binding setup resembling the current pattern in Chern insulator setup (1D wire is between 0-50. 2D reservoirs are between -150-0 and 50-200)

in the tight binding setup at $\mu = 0$. Darker shade represents higher magnitude of current. This figure is directly obtained using KWANT python package. Here, the current pattern in the left reservoir has more magnitude because of the reflection happening at the left junction ($x = 0$).

Chapter 7

Conclusion

In this report, we studied a model for Chern insulator (spinless BHZ) coupled to metallic leads at its two ends (we call it an open system). This is a typical setup for transport experiments for conductance measurements. Considering a cylindrical geometry for this setup, we derived an analytic expression for Hall conductance using Non-Equilibrium Green's Function (NEGF) formalism. Our expression for Hall conductance in an open system setup shows that it is indeed quantized, independent of the details of coupling of Chern insulator to metallic leads. This is analytically shown in the weak coupling limit. The derived expression for Hall conductance has an integral form in the thermodynamic limit ($N_x, N_y \to \infty$), suggesting a possible connection to some topological invariant. Note that the goal of deriving such an expression was to obtain a similar result to TKNN expression (Thouless *et. al.* 1982 [5]) where they proved that Hall conductivity of a *closed periodic* system can be expressed in terms of Chern number (a topological invariant) of filled bands which explained the robustness of quantized conductance to disorders. By contrast, our open system perspective using NEGF formalism hopes to clarify why conductance is quantized even in the presence of metallic leads(reservoirs) where the details(coupling) at the junction of system and reservoir affects the transport properties. Although our analytic expression is shown to be quantized in the weak coupling limit, its connection to some topological invariant is still not obtained by us.

Apart from our expression for Hall conductance, we also numerically studied the finite strip geometry setup of the spinless BHZ model connected to 2D metallic leads using NEGF formalism and KWANT python package. Our numerical results in this setup helped to under-

stand the reason behind oscillations in two terminal conductance observed in reference [13]. Using these insights, we understood the role of real and imaginary part of the self energy term in effective Hamiltonian of the setup. This lead us to consider a simpler model for reservoir using which we get rid of the oscillations. We also numerically showed that the current pattern observed(inside metallic leads) in Chern insulator setup at $\mu = 0$ in reference [13] can also be obtained in a simple tight binding setups without any non-trivial topology. In addition to spinless BHZ model, we also verified the quantization of two-terminal conductance in Hofstadter model where the conductance was observed to quantize at 1 and/or 2 (depending on the flux parameter).

In summary, our analytic derivation confirms that the Hall conductance remains quantized in the thermodynamic limit, thereby supporting the perfect transmission assumption inherent in the Landauer–Büttiker formalism for topological systems. Our numerical analysis using a finite strip geometry elucidates the critical role of the reservoir's self-energy in shaping the conductance behavior of the Chern insulator setup. Overall, this work lays a theoretical foundation for understanding topological systems in an open system setup, providing valuable insights that can can possibly guide and optimize experimental strategies for the realization of two-dimensional topological insulators.

Appendix A

Fourier transforming SBHZ Hamiltonian and self energy using unitary matrix

In this appendix, we explicitly show that the single particle Hamiltonian and the self energy matrices are block diagonal if a Fourier transformation is done along $y-$direction using the unitary matrix.

A.1 Unitary transformation of SBHZ Hamiltonian

The Hamiltonian for the SBHZ model in matrix form is given by:

$$H_{x,y;x',y'} = \delta_{x,x'}\delta_{y,y'}V \qquad \text{Part I} \tag{A.1}$$

$$+ \delta_{y,y'}\delta_{x,x'-1}A + \delta_{y,y'}\delta_{x,x'+1}A^{\dagger} \qquad \text{Part II} \tag{A.2}$$

$$+ \delta_{x,x'}\delta_{y,y'-1}B + \delta_{x,x'}\delta_{y,y'+1}B^{\dagger} \qquad \text{Part III} \tag{A.3}$$

Here, V, A, B are 2×2 matrices representing site potential, hopping in x-direction and hopping in y direction respectively. In Part III we assume periodic boundary condition, i.e

$y = 0 = N$ and $y = N + 1 = 1$. Applying unitary transform on the Hamiltonian, we get

$$(U^\dagger HU)_{x,y;x',y'} = \sum_{x_1,y_1} \sum_{x_2,y_2} (U^\dagger)_{x,y;x_1,y_1} (H)_{x_1,y_1;x_2,y_2} (U)_{x_2,y_2;x',y'} \tag{A.4}$$

For simplicity, we will apply the Unitary transform on Part I, II and III separately:

Part-I:

$$\sum_{x_1,y_1} \sum_{x_2,y_2} (U^\dagger)_{x,y;x_1,y_1} (\delta_{x_1,x_2}\delta_{y_1,y_2} V) \;\; (U)_{x_2,y_2;x',y'} \tag{A.5}$$

$$= \frac{1}{N_y} \sum_{x_1,y_1} \sum_{x_2,y_2} (e^{-ik_y y_1}\delta_{x_1,x_2}) \; (\delta_{x_1,x_2}\delta_{y_1,y_2} V) \; (e^{ik_{y'} y_2}\delta_{x',x_2}) \tag{A.6}$$

$$= \frac{1}{N_y} \sum_{y_1} e^{-i(k_y - k_{y'})y_1} \delta_{x,x'} V \tag{A.7}$$

$$= \delta_{x,x'}\delta_{y,y'} V \tag{A.8}$$

Part-II:

$$\sum_{x_1,y_1} \sum_{x_2,y_2} (U^\dagger)_{x,y;x_1,y_1} (\delta_{y_1,y_2}\delta_{x_1,x_2-1} A + \delta_{y_1,y_2}\delta_{x_1,x_2+1} A^\dagger) \;\; (U)_{x_2,y_2;x',y'} \tag{A.9}$$

$$= \frac{1}{N_y} \sum_{x_1,y_1} \sum_{x_2,y_2} (e^{-ik_y y_1}\delta_{x_1,x_2}) \; (\delta_{y_1,y_2}\delta_{x_1,x_2-1} A + \delta_{y_1,y_2}\delta_{x_1,x_2+1} A^\dagger) \; (e^{ik_{y'} y_2}\delta_{x',x_2}) \tag{A.10}$$

$$= \frac{1}{N_y} \left(\sum_{x_1,y_1} e^{i(k_y - k_{y'})y_1} \delta_{x,x_1}\delta_{x',x_1-1} A^\dagger + \sum_{x_1,y_1} e^{i(k_y - k_{y'})y_1} \delta_{x,x_1}\delta_{x',x_1+1} A \right) \tag{A.11}$$

$$= \delta_{y,y'}\delta_{x,x'+1} A^\dagger + \delta_{y,y'}\delta_{x,x'-1} A \tag{A.12}$$

Part-III:
$$\sum_{x_1,y_1}\sum_{x_2,y_2}(U^\dagger)_{x,y;x_1,y_1}(\delta_{x_1,x_2}\delta_{y_1,y_2-1}B+\delta_{x_1,x_2}\delta_{y_1,y_2+1}B^\dagger)\ \ (U)_{x_2,y_2;x',y'} \tag{A.13}$$

$$=\frac{1}{N_y}\sum_{x_1,y_1}\sum_{x_2,y_2}(e^{-ik_y y_1}\delta_{x_1,x_2})\ (\delta_{x_1,x_2}\delta_{y_1,y_2-1}B+\delta_{x_1,x_2}\delta_{y_1,y_2+1}B^\dagger)\ (e^{ik_{y'}y_2}\delta_{x',x_2}) \tag{A.14}$$

$$=\frac{1}{N_y}\left(\sum_{y_1}\delta_{x,x'}e^{-ik_y y_1}e^{ik_{y'}(y_1+1)}B+\sum_{y_1}\delta_{x,x'}e^{-ik_y y_1}e^{ik_{y'}(y_1-1)}B^\dagger\right) \tag{A.15}$$

$$=\frac{1}{N_y}\left(N\delta_{x,x'}\delta_{y,y'}e^{ik'_y}B+N\delta_{x,x'}\delta_{y,y'}e^{-ik'_y}B^\dagger\right) \tag{A.16}$$

$$=\delta_{x,x'}\delta_{y,y'}(e^{ik'_y}B+e^{-ik'_y}B^\dagger) \tag{A.17}$$

$$\tag{A.18}$$

Combining the 3 parts, the unitary transformed Hamiltonian $(\tilde{H})_{x,y;x',y'}=(U^\dagger HU)_{x,y;x',y'}$ comes out to be:

$$\boxed{(\tilde{H})_{x,y;x',y'}=\left[\delta_{x,x'}(V+e^{ik_y}B+e^{-ik_y}B^\dagger)+\delta_{x,x'+1}A^\dagger+\delta_{x,x'-1}A\right]\delta_{y,y'}} \tag{A.19}$$

Note that $\delta_{y,y'}$ outside bracket tells us that $\tilde{H}$ can be thought of as a block diagonal matrix in some basis.

A.2 Unitary transformation of self energy

Self energy adds imaginary site potential to all the $x=1$ and $x=N_x$ sites. Hence the matrix for self energy is of the form:

$$\Sigma_{x,y;x',y'}=\frac{-i\eta_c^2}{\eta_b}\ \ \delta_{y,y'}\delta_{x,x'}\delta_{1,x'}\delta_{N_x,x'} \tag{A.20}$$

Applying unitary transform, we see that

$$(U^\dagger \Sigma U)_{x,y;x',y'} = \sum_{x_1,y_1}\sum_{x_2,y_2}(U^\dagger)_{x,y;x_1,y_1}\Sigma_{x_1,y_1;x_2,y_2}U_{x_2,y_2;x',y'} \tag{A.21}$$

$$= \frac{-i\eta_c^2}{\eta_b}\sum_{x_1,y_1}\sum_{x_2,y_2}\frac{1}{N_y}(e^{-ik_y y_1}\delta_{x_1,x})\ (\delta_{y_1,y_2}\delta_{x_1,x_2}\delta_{1,x_1}\delta_{N_x,x_1})\ (e^{ik_{y'}y_2}\delta_{x',x_2}) \tag{A.22}$$

$$= \frac{-i\eta_c^2}{\eta_b}\frac{1}{N_y}\sum_{y_1}e^{i(k_{y'}-k_y)y_1}\delta_{x,x'}\delta_{1,x}\delta_{N_x,x} \tag{A.23}$$

$$= \frac{-i\eta_c^2}{\eta_b}\delta_{y,y'}\delta_{x,x'}\delta_{1,x}\delta_{N_x,x} \tag{A.24}$$

$$= \Sigma_{x,y;x',y'} = \tilde{\Sigma}_{x,x'}\ \ \delta_{y,y'} \tag{A.25}$$

where we define 1D self energy, $\tilde{\Sigma}_{x,x'} = \frac{-i\eta_c^2}{\eta_b}\delta_{x,x'}\delta_{1,x}\delta_{N_x,x}$. So, **self energy remains unchanged under unitary transform** and it's x and y indices are uncoupled.

$\Gamma_{L/R}$ is defined as $\frac{\Sigma_{L/R}^\dagger - \Sigma_{L/R}}{2\pi i}$. From the above calculation, it is clear that $\Gamma_{L/R}$ is block diagonal if written in matrix form. Hence, we have ($\Gamma = \Gamma_{L/R}$)

$$\boxed{\Gamma_{x,y;x',y'} = \tilde{\Gamma}_{x,x'}\ \ \delta_{y,y'}} \tag{A.26}$$

$\tilde{\Gamma}$ is the imaginary part of 1D self energy.

Bibliography

[1] Joel E Moore. The birth of topological insulators. *Nature*, 464(7286):194–198, 2010.

[2] K. von Klitzing, G. Dorda, and M. Pepper. New method for high-accuracy determination of the fine-structure constant based on quantized hall resistance. *Phys. Rev. Lett.*, 45:494, 1980.

[3] David Tong. Lectures on the quantum hall effect, 2016. Lecture notes.

[4] Robert B Laughlin. Quantized hall conductivity in two dimensions. *Physical Review B*, 23(10):5632, 1981.

[5] D. J. Thouless, M. Kohmoto, M. P. Nightingale, and M. den Nijs. Quantized hall conductance in a two-dimensional periodic potential. *Phys. Rev. Lett.*, 49:405, 1982.

[6] F. D. M. Haldane. Model for a quantum hall effect without landau levels: Condensed-matter realization of the "parity anomaly". *Phys. Rev. Lett.*, 61:2015, 1988.

[7] C. L. Kane and E. J. Mele. Z_2 topological order and the quantum spin hall effect. *Phys. Rev. Lett.*, 95:226801, 2005.

[8] B. A. Bernevig, T. L. Hughes, and S.-C. Zhang. Quantum spin hall effect and topological phase transition in hgte quantum wells. *Science*, 314:1757, 2006.

[9] B. Andrei Bernevig and Taylor L. Hughes. *Topological Insulators and Topological Superconductors*. Princeton University Press, 2013.

[10] J. M. Bhat and A. Dhar. Equivalence of NEGF and scattering approaches to electron transport in the kitaev chain, 2023. arXiv preprint.

[11] Abhishek Dhar and Diptiman Sen. Nonequilibrium green's function formalism and the problem of bound states. *Physical Review B—Condensed Matter and Materials Physics*, 73(8):085119, 2006.

[12] M. König, S. Wiedmann, C. Brüne, A. Roth, H. Buhmann, L. W. Molenkamp, X.-L. Qi, and S.-C. Zhang. Quantum spin hall insulator state in hgte quantum wells. *Science*, 318:766, 2007.

[13] J. M. Bhat and A. Dhar. Quantized two terminal conductance, edge states and current patterns in an open geometry 2D chern insulator, 2023. arXiv preprint.

[14] J. M. Bhat. Topologically protected subdiffusive transport in two-dimensional fermionic wires. *Phys. Rev. B*, 109:125415, 2024.

[15] D. J. Griffiths. *Quantum Mechanics*. Cambridge University Press, third edition, 2018.

[16] Christoph W Groth, Michael Wimmer, Anton R Akhmerov, and Xavier Waintal. *Kwant: a software package for quantum transport. New Journal of Physics*, 16(6):063065, 2014.

[17] Supriyo Datta. *Quantum Phenomena*. Addison-Wesley, Reading, MA, 1989.

[18] Yasuhiro Hatsugai. Edge states in the integer quantum hall effect and the riemann surface of the bloch function. *Physical Review B*, 48(16):11851, 1993.